POLITECNICO DI TORINO

Master's Degree Course in Biomedical Engineering

Master's Degree Thesis

Analysis of piezoionic phenomenon in hydrogel materials and implementation for the fabrication of innovative self-powered tactile sensors

Academic year 2023-2024

Supervisor:

PROF. Stassi Stefano

Author:

Arias Belduque Maria José

Abstract

Nowadays many of the sensors used in the market take advantage of the characteristic physical behaviours of some materials to develop new devices. The piezoionic phenomenon is an effect in which applying pressure on the material generates a redistribution of ions that can be translated into a voltage and current output. This physical mechanism can be useful to describe the sensory behaviour of the skin, so its study can lead to the creation of new self-powered sensors and Smart skins as well as new robotic and prosthetic applications. This study analyses the piezoionic effect in a semi-interpenetrated polymeric network hydrogel. The impact of ionic mobility on the electrical response of the material was validated using salts with the same anion but different cation. Samples with parallel and sandwich copper electrodes were subjected to various tensile and compression tests to evaluate the electrical behaviour of the different mobile ions. In addition, the response in time to a constant force was studied to analyse the diffusivity of the ions. After the functional characterization of the material, the hydrogel was implemented as a biometric self-powered sensor for human movement. With the results obtained it has been possible to establish this type of hydrogels as an alternative to develop new tactile sensors that allow the perception of the skin as well as innovative devices useful in soft robotics, energy harvesting and biomedicine.

CONTENTS

List of Tables

List of Figures

Chapter 1.

Introduction

For years, science has relied on nature to mimic the structure and functions of the human body artificially. The sense of touch is what enables people to interact with their surroundings and react differently to various stimuli. The largest organ in the human body, the skin, contains mechanoreceptors that are activated by external stimuli. These receptors allow the skin to function as a sensor. Lack of tactile perception has prompted researchers to look for and develop new devices that use various sensor types to replicate how the skin functions. The most popular types are piezoresistive, piezocapacitive, piezoelectric, and triboelectric sensors, however, piezoionic sensors, which function by producing an internal ionic motion that can be translated into an electrical response when a mechanical stimulus is applied, have only recently been studied and put into practise. These sensors major advantage is that they are self-powered and do not require an external source to produce current or voltage, in addition, their sensory behaviour is comparable to that of skin. On the other hand, tactile sensors are typically made of materials that enable them to structurally and functionally mimic human skin, as a result, soft, flexible materials must be used in the construction of these devices. These properties, along with their high biocompatibility and ionic sensitivity, are what define hydrogels. Their characteristics enable their extensive application in the domains of soft robotics and electronic skin.

In order to analyse the piezoionic phenomenon, a tactile sensor consisting of a hydrogel made of an aqueous solution of polyvinyl alcohol (PVA), acrylic acid (AAc), and polyethylene glycol diacrylate (PEGDA) was created. The hydrogel was curable under UV light. A review of the most recent developments in the field of tactile perception is given first, along with an overview of the primary sensor types employed in this field. Hydrogels and their classification system are also discussed. Lastly, some new uses for touch sensors are discussed. The sensor's development and manufacturing process, as well as the tools and supplies utilised for the project, are then described. The comprehensive electrical and mechanical characterization of the sensor is presented in the results. Several salts were employed in the material's synthesis to investigate ionic mobility and how it affected the electrical response, in this instance, the cations were altered with various alkali metals, but the anion of chlorine (Cl) stayed constant. After the polymer had cross-linked, copper electrodes were integrated into two conformations: one parallel and the other sandwich-shaped. To assess the electrical response of the different ions, both types of samples underwent various compression and stress tests. During trials, the Keithley measuring device was used to measure voltage and current. The response of ionic mobility over time was found by applying a constant force for a specified amount of time. Lastly, the sensor was employed to measure a range of human activities. Based on the results, it was possible to show that the internal redistribution of ions in the piezoionic polymeric sensor allows it to generate an electrical signal output when subjected to mechanical deformation. It was also demonstrated that this sensor could have applications in the biomedical field, including wearable sensing and the development of electronic skins.

Chapter 2.

State of the art

2.1. Tactile perception

Skin is an organ that covers the entire body surface, its structure is composed of three different layers: the *epidermis*, a thin, elastic, avascular and superficial layer, the *dermis*, a bilayer that contains connective tissue, blood, nerves, hair follicles and sweat glands and the *hypodermis* which is the deeper layer that houses adipose lobules along with some sensory neurons and blood vessels (Figure 2.1) [1].

This hierarchical and multicellular structure serve as a protective barrier that allows interaction with the outside world and enables the body to discriminate objects and surfaces as well as to perceive various stimuli from the environment like temperature, pressure, or humidity [2].

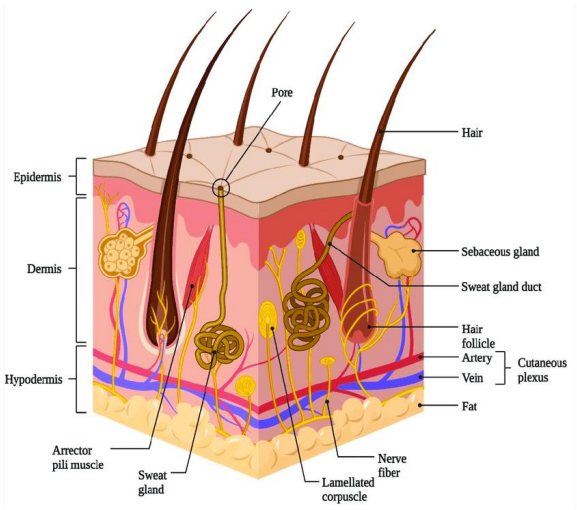

Figure 2.1. *Human skin structure and components [3]*

The ability to perceive and discriminate through touch is possible thanks to the sensory receptors found on the skin called mechanoreceptors, this are neurons of different types and each respond in a unique way to a stimulus, the Pacinian corpuscles are located deep in the tissue and are responsible for vibration detection, Ruffini's corpuscles identify skin stretch and are present within the dermis layer, the Meissner corpuscles are stimulated by skin motion and are located in the epidermis layer and the Merkel cells are in the epidermis and respond to light touches [4] Nerves and connective tissue surround these structures and they have a distinct region of stimulation known as the receptive field. When the stimulus is received, the mechanoreceptor activates and responds, producing an electrical signal [5] Nevertheless, the tactile perception is a process more complex that it seems, it involves a

whole chemical interaction and a strong communication with Central Nervous System (CNS).

The sensory transduction starts with the reception of the external stimuli in the receptive field of the mechanoreceptors, this physical disturbance leads to the opening of the ionic channels and an ion movement from one side of the membrane to the other as it shows in Figure 2.2. This mechanical induced ionic current produces a variation in the membrane potential [6]

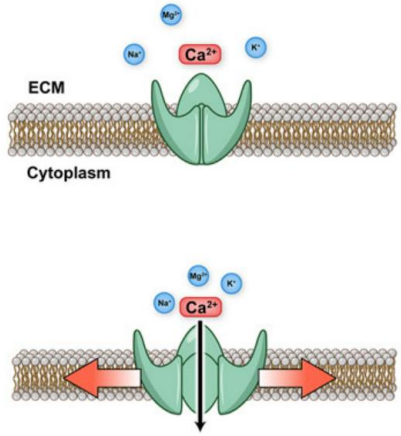

Figure 2.2. *Closure and opening of the ion channels of the cell membrane [7]*

In normal conditions, the cell membrane potential is negative and about -70mV, when the stimulus is high enough and exceed a threshold, there's a conformation change that guides to the opening of the channel and produce a positive depolarization of the membrane to which the neuron responds with a receptor or action potential. Eventually, the channels begin to close, and the potential diminishes until its resting state [8] [8] A typical curve of the action potential of a cell membrane is illustrated in Figure 2.3.

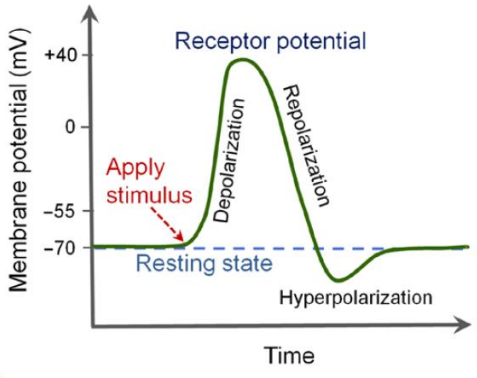

Figure 2.3. *Typical neuronal action potential curve in response to a stimulus [6] .*

Action potentials lead to the activation of different signal pathways with specific effects on cell behaviours. These are sent in response to mechanical stimuli through type II A fibres as a train of impulses, this signal information travels to the thalamus, then synapses in the dorsal spinal cord, and ultimately arrives to the somatosensory cortex for central processing and interpretation, in this way, humans develop the sense of touch and therefore, the body can perceive different objects and surfaces (Figure 2.4) [1].

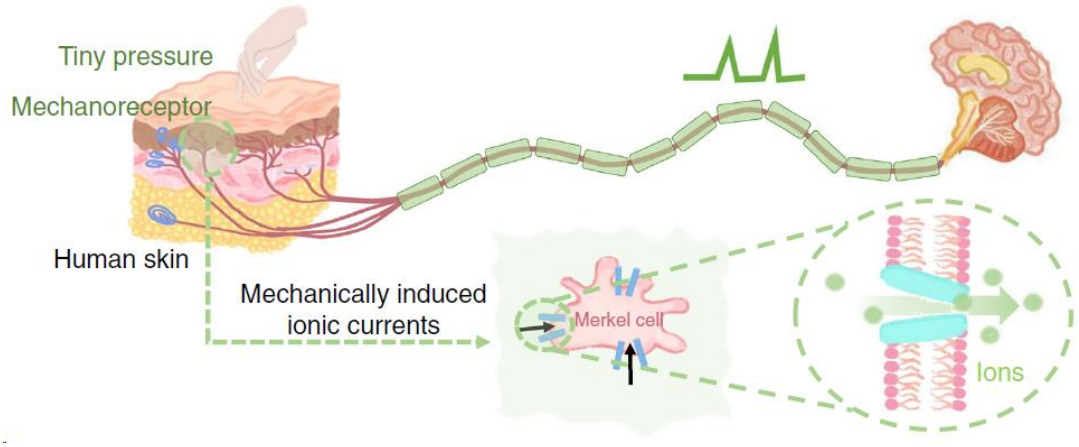

Figure 2.4. *Mechanically gated tactile-sensing mechanism of human skin [9] .*

The mechanosensitive Piezo1 and Piezo2 ion channels, which are widely expressed in various vertebrate tissues and are in charge of sensing mechanical stimulations, were found in 2010 in a cell culture that was exposed to a potent mechanically induced current. These channel proteins are crucial for many physiological and pathological processes, including mechanosensation and mechanotransduction. Because of them, humans are able to recognise and react to a variety of stimuli [10] . David Julius and Ardem Patapoutian were awarded the Nobel Prize in Physiology or Medicine in 2021 for their research on temperature and touch receptors. Their work involved analysing and comprehending the atomic structure of Piezo1 and Piezo2 channels [11] Their findings have contributed to understand the physiological and biologic processes involved in human perception of environmental stimuli, as well as the exploration of novel approaches for the development of ionic skins and artificial senses of touch.

2.2. Sensors

Sensors have been crucial in a wide range of medical applications, its implementation has led to the development of more complex devices and the study of biological processes and pathologies. Instead of translating the information into nerve impulses, sensors translate them into electrical signals. These instruments are utilized to sense the physical properties of an environment and turn them into an output signal that can be measured, recorded, or integrated into another circuit to finally undergo into a processing phase.

When comparing the sensor's input and output, these instruments have specifications that show potential sources of uncertainty or error limits. They are distinguished by their repeatability, precision, and resolution, and they feature a measuring range with a minimum and maximum limit to provide a precise response. As a result, the output shouldn't change until a specific input increment is exceeded. It also needs to be linear to enable value conversion and keep sensitivity constant.

There are various types of sensors because they each contain a unique signal conditioning unit that enables the conversion of an input into an electrical output based on the phenomenon to be monitored. Biosensors, for example, are instruments that use a biological detecting element to find out whether a biomolecule, an organic structure, or a microorganism is present or concentrated. In order to create a biosensor with a highly sensitive, quick, and easy way to detect the virus during the pandemic, Seo et al. connected the SARS-CoV-2 antibody to a graphene sheet (Figure 2.5). Without any prior treatment, the sensor was able to identify the SARS-CoV-2 virus in clinical samples [12] . This instrument may be used to do immunological diagnostics of more newly discovered viral illnesses.

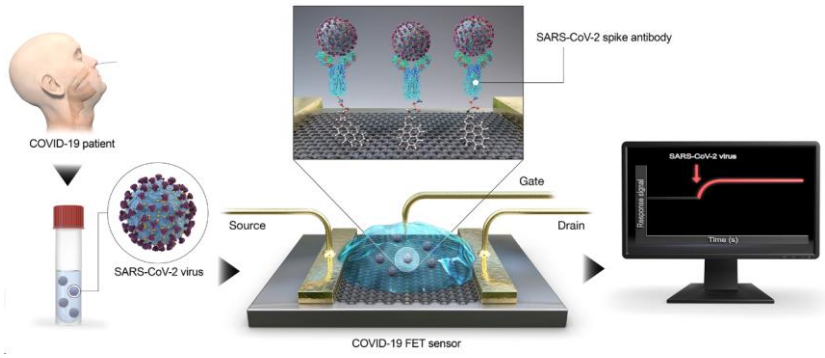

Figure 2.5. *Schematic diagram of COVID-19 biosensor operation procedure. A layer of graphene is used to bind the SARS-CoV-2spike antibody to detect the virus in preclinical samples [12]*

Sensors are incredibly versatile devices that may be adjusted based on a variety of factors, including their operating principle, energy requirements, composition, and output type. Characterised by their capacity to use various transduction methods, tactile sensors can translate an external mechanical stimulation into an electrical output. By contacting a surface, identifying shapes and textures, or detecting various forces, these sensors react to

physical interactions from the surroundings. The way tactile sensors work can be used to categorise them. While passive sensors do not require an external source to function and do not directly regulate electrical signals, active sensors do require an external source to be able to transmit energy, produce signals and measure their reflection. Although both types of sensors are widely used, which one is used depends on the kind of information that needs to be acquired or the application that needs to be developed. Piezoresistive, capacitive, piezoelectric, triboelectric, and the newest piezoionic sensors are some of the most widely used types of sensors, especially for electronic skins and human-machine interfaces.

2.2.1. Piezoresistive sensors

Piezoresistive effect is based on a change in the resistance of a material when a mechanical stimulus is applied. This phenomenon can be reflected through the changes in an electrical output (Figure 2.6). This type of behaviour is typical of conductive materials, which exhibit a resistance (R), an opposition to the flow of electric current. As equation 2.1 illustrates, this property can be mathematically expressed as the resistivity (ρ), the length (L), and the cross-sectional area of the conductor (A). Consequently, modifications to the material's resistivity or geometry may result in variations in electrical resistance. These are examples of active sensors because in order for them to produce a response, they require an external voltage source.

$$R = \frac{\rho L}{A} \tag{2.1}$$

The gauge factor (G), which is the ratio of the fractional change in electrical resistance to the change in strain (ε), can be used to express the sensitivity of this type of sensors. The gauge factor in the limit of low strain is defined in Equation 2.2. In this instance, R_0 represents the resistance measured in the absence of a stimulus, and ΔR represents the variance between R and R_0. Different materials have different G values [13] . For instance, metal foil strain sensors typically have low values between 2 and 4, while semiconducting and softer materials can have higher values. However, an elevated gauge factor may result in inferior performance of other properties like hysteresis and linearity.

$$\frac{\Delta R}{R_0} = G\varepsilon \tag{2.2}$$

Around 1950, strain gauges made of metallic foils were invented, marking the beginning of the development of devices that used the piezoresistive effect [14] These sensors were employed to measure strain in various surfaces and structures by utilising a change in geometry and their piezoresistive behaviour. These gauges are typically made of nickel and copper alloys because of their high resistivity and strain sensitivity, but they also have high power consumptions, permanent drift at certain temperatures, and a tendency for the measure to not stabilise over time [15] [16] Semiconductors gained popularity in the late 20th century for use in the development of sensing and measuring devices across a wide range of industries, germanium and silicon were particularly used [17] The applied force in

semiconductive materials causes the charge carriers to move, altering the energy band-gap. As a result, the resistivity change depends on the density and mobility of these load carriers [18]

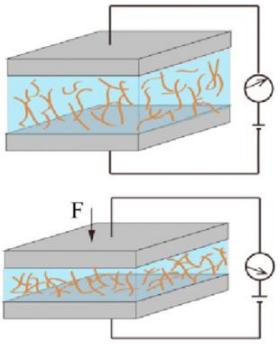

Figure 2.6. *Piezoresistive transduction mechanism [18]*

Two common semiconductors are graphene and carbon nanotubes (CNTs). Excellent mechanical qualities, stability, flexibility, and high intrinsic carrier mobility characterise these materials. A highly sensitive pressure sensor for vertical forces within the range of human perception was created by Chun et al. Two independent single-layered graphenes were used to create the device, and they were supported by a flexible polydimethylsiloxane (PDMS) substrate (Figure 2.7). Two modes of resistance change sensitivity are enabled by the design configuration: a low pressure mode ($-0.24\ kPa^{-1}$) and a high pressure mode ($0.039\ kPa^{-1}$). This sensor can identify the surface morphology of the contacting materials and detect minuscule pressures as low as 0.3 Pa when a uniform vertical force is applied [19] During the study was demonstrated the use of the sensor in the monitoring of human activities with a measure of the pulse beat.

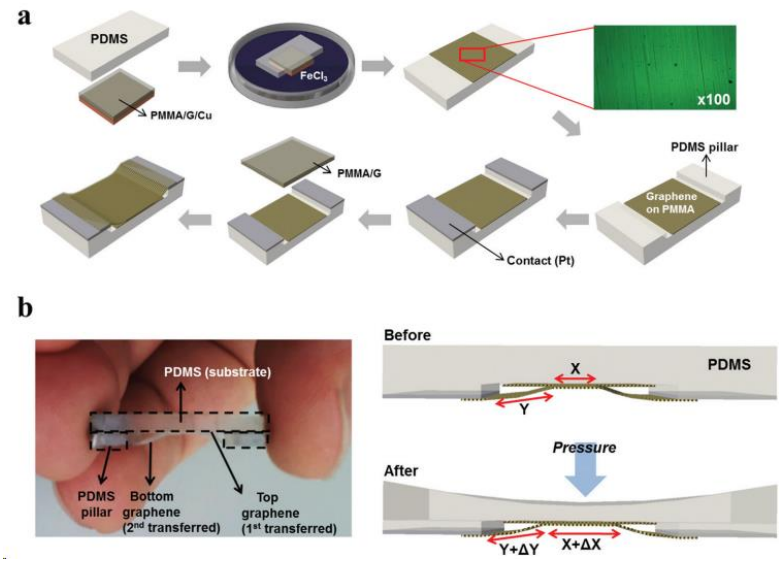

Figure 2.7. *(a) Process of graphene and PDMS sensor formation. (b) Built-in pressure sensor photography (left) and schematic mechanism of operation under the application of a vertical force (right) [19]*

Although the development of tactile sensors has traditionally relied on semiconductors, recently there has been a shift towards the use of more flexible, deformable materials that are easily adapted to irregular surfaces. The combination of an active substance and a substrate is known as a conductive compound. The most common active materials are graphene, metal nanoparticles, and carbon nanotubes. They also typically have good mechanical and electrical properties. However, the substrate provides the sensor with flexibility and softness, for this reason, hydrogels or polymers are utilised [18] . Polyethylenes (PE), polyurethanes (PU), and PDMS are a few examples of substrate materials. These sensors are highly biocompatible with the human body and can have extremely high gauge factor values. For instance, a conductive composite with carbon nanotubes embedded in the matrix of nano porous PDMS sponges was created by Herren et al. in 2021. In order to maximise conductivity and sensitivity to compression while maintaining the material's mechanical qualities, the researchers employed microwave irradiation to adjust the sponge's porosity, change its hardness and strength, and determine the ideal number of CNTs. In this work, various porosity sponges underwent compression tests. The least porous material inside the sponge, with 3% NTC, had the highest compressive sensitivity, which was between 5% and 50% strain [20] . Following its characterization, this sponge was employed as a sensor for various human movement functions, such as breathing, walking, running, and elbow flexion. It was also used to measure compression on a prosthetic hand finger, as illustrated in Figure 2.8.

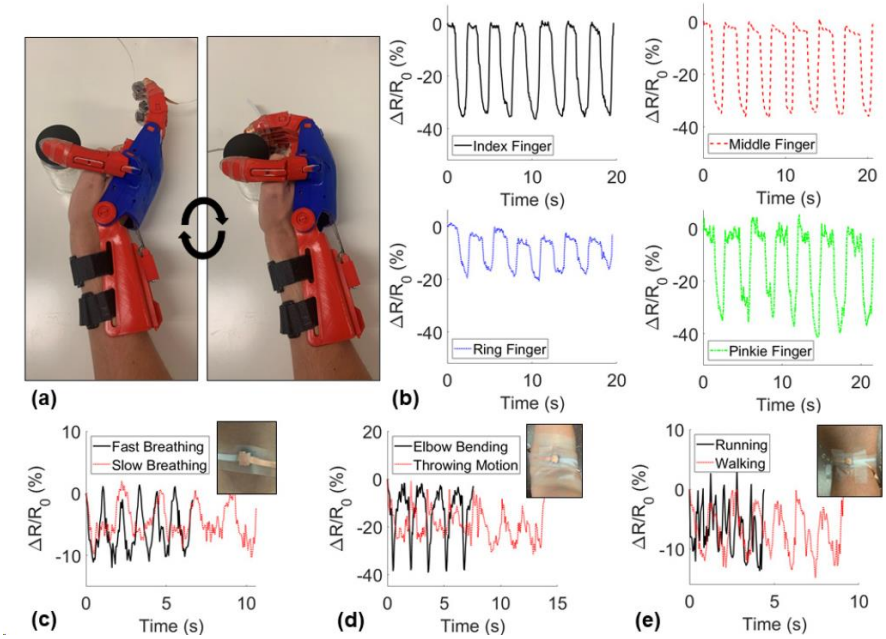

Figure 2.8. *Applications of sponge sensors: (a-b) fingertip pressure detection on a prosthetic hand and detection of human movements like (c) breath monitoring (d) elbow bending, and (e) running and walking [20]*

The dynamic percolation or quantum tunnelling mechanism in conductive composites is a manifestation of the piezoresistive phenomenon, which is contingent upon the polymer's filler content. When the filler concentration is low, the particles are scattered throughout the matrix, resulting in a high electrical resistance, as the filler concentration rises, the resistance decreases, and a conductive path is formed between the particles (Figure 2.9) [14]

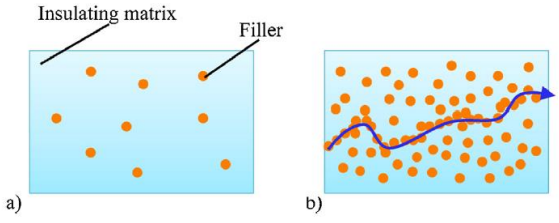

Figure 2.9. *Illustration of the dynamic formation of the conductive path due to percolation in polymers during (a) filler low concentration and (b) high filler concentration [14]*

The conductivity (σ) of the polymer can be used to express the dynamic percolation, as demonstrated by the following equation:

$$\sigma = \sigma_0 \, (V_f - V_c)^s \tag{2.3}$$

where σ_0 corresponds to a proportionality constant of the filler conductivity, V_f is the volume fraction of the filler, V_c is the percolation threshold and s is the conductivity exponent which depends on the material characteristics.

Piezoresistive sensors are highly used by their convenient fabrication process, they are easy to integrate, have low power consumption and are less affected by cross-talk or noise [21].

Their major limitations are their low sensitivity to small strain changes, resistance hysteresis and their degradation by fatigue [22] .

2.2.2. Capacitive sensors

A capacitor consists of two conductive surfaces that are separated by a dielectric material. These devices are used to store energy as an electrical charge. This stowage capacity is known as capacitance (C), which is expressed as:

$$C = \frac{\varepsilon_r \varepsilon_0 A}{d} \tag{2.4}$$

where ε_0 is the permittivity of free space, ε_r is the relative static permittivity of the dielectric layer, A is the area of the overlap of the two plates, and d is the distance between conductive surfaces. Capacitors can act as a piezocapacitive sensors, producing an electrical signal in response to a change in capacitance brought on by an external mechanical stimulus, according to the geometric parameters A and d, which are changeable by forces or pressures (Figure 2.10). ε_r can be used to identify forces in microstructured materials or with embedded fillers, whereas the area is used to measure shear forces and strains and the distance is used to measure normal forces [21] [23]

The relationship between the capacitance change (ΔC) and the starting capacitance before providing a stimulus (C0), as well as the pressure applied to the sensor (ΔP), define the sensitivity of a piezocapacitive sensor. This relationship is illustrated in the following equation:

$$S = \frac{(\Delta C / C_0)}{\Delta P} \tag{2.5}$$

Since the sensitivity is heavily dependent on the dielectric layer, researchers aim to use materials with sufficient viscoelasticity and minimise its elastic resistance [24] Lately, the utilisation of porous structures and malleable and conductive materials has been determined [25] Examples of such materials are polymer substrates, sponges, foams, and elastomers that contain conductive nanostructures.

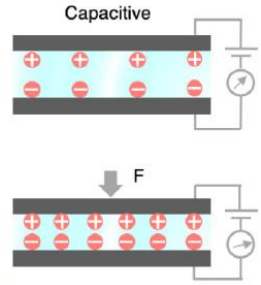

Figure 2.10. *Capacitive transduction mechanism [21].*

In order to design a highly sensitive and deformable piezocapacitive sensor, Baek et al. used a soft dielectric made of a biodegradable silicone called Ecoflex, compress between two layers of copper to form the electrodes. After the Ecoflex was treated with ultraviolet-ozone to solidify it, the forces were released, resulting in the microstructured wrinkled surface depicted in Figure 2.11. This architecture allows reversible storage and release of energy after an external force is applied [25] Using this device, scientists were able to identify three different kinds of mechanical forces by the change in capacitance (object loading and unloading, pressure in the mouth during an exhaled breath, and the induced compression to open a book and the angle of the stimulus). These were all detected by the change in capacitance.

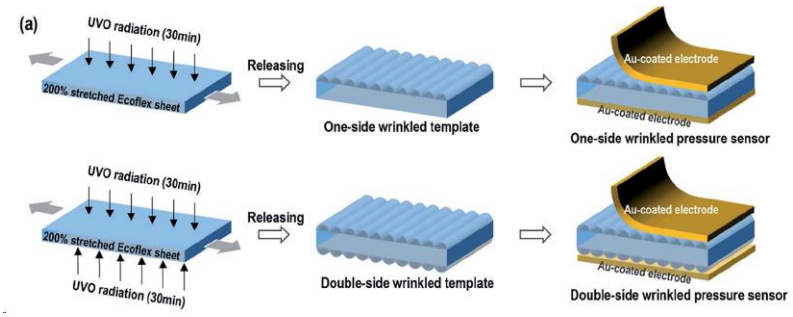

Figure 2.11. *Schematic of the wrinkled Ecoflex pressure sensor manufacturing process [25]*

Yoon et al. created another example of a piezocapacitive sensor. Using an irregular layer of conductive PDMS elastomers and carbon nanotubes sandwiched between two gel films holding an ionic liquid, researchers from the University of Seoul were able to create a sensor that could detect both dynamic and static pressures. The sensor features stability, a response time of less than 52 ms, a low detection limit of less than 5 Pa, a low working voltage of 0.1 V, and high sensitivity of 9.55 kPa^{-1}. Various physiological parameters were identified throughout the sensor test [26] . The sensor was applied to the patient's neck in the vicinity of the carotid artery (Figure 2.12b) in order to detect the diastolic and systolic pressure and monitor the artery's pulses as it shows in Figure 2.12c. In addition, gulping could be distinguished as well as deep breathing (Figure 2.12d).

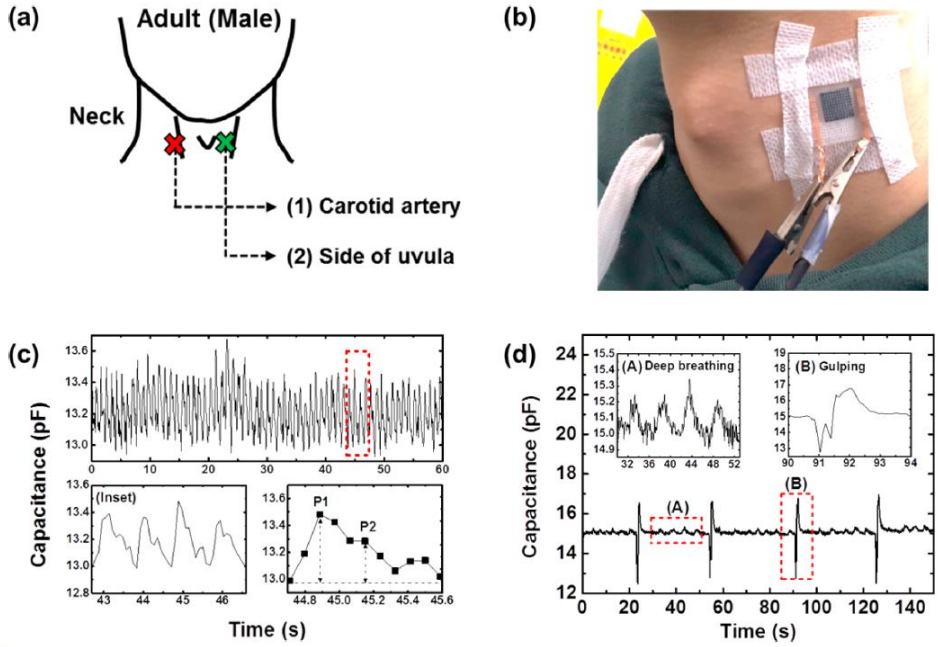

Figure 2.12. *(a) Schematic of neck for monitoring of human physiological signals. (b) Photography of the pressure sensor on the carotid artery. (c) Pulse measurements on the carotid artery with the capacitive pressure sensor and (d) detection of a deep breath and gulping signals [26]*

Since they use less energy and have a high sensitivity, flexible piezocapacitive sensors have been researched extensively in the field of tactile sensors. Measurements without direct contact can also be made using the cumulative load on the plates [24] But there are still certain areas where these devices need to be improved. For example, they tend to lose their linearity and are prone to interference from nearby objects that could distort the output signal.

2.2.3. Piezoelectric sensors

Piezoelectric sensors are another widely investigated type of tactile sensors. When a material undergoes mechanical deformation, these devices produce an electrical potential. As demonstrated in Figure 2.13, the effect also operates conversely. When an alternating potential difference is supplied, the material may deform or oscillate at a particular frequency and amplitude [27] . This phenomenon was initially identified in 1880 by Jacques and Pierre Curie in anisotropic crystals. As a result of these materials' lack of centres of symmetry, charges are produced on opposing surfaces when a mechanical stimulus is provided, dipoles are oriented, and an electrical polarisation happens in the force's direction [28] Unlike resistive and capacitive sensors, piezoelectrics have the ability to work without an external source of energy, so they are known as self-powered sensors. Ceramic materials like zirconia, zinc, and titanium exhibit the piezoelectric action, nevertheless, their extremely high Young modules exclude their use in the creation of touch sensors [21]. Under such circumstances, polymers could be used because they are more flexible, biocompatible, soft, and have low production costs. However, the drawback of polymers is that they don't have piezoelectric coefficients as high as ceramics. Thus, today's applications include

piezoelectric sensors based on polymer matrices and inorganic material composition. Throughout their research, Bentoholda and colleagues developed a sensor that could perform biomedical monitoring of various biological signals incorporating microporous zirconium-based metal–organic frameworks (MOFs) on a poly(vinylidene fluoride) (PVDF) nanofibrous membrane. Using the electrospinning method, the polymer solution and nanoparticles were combined to create the fibres. A voltage differential between a conductive mounting tip and the samples was used to study the piezoelectric response of the sensor using the Atomic-force microscopy (AFM) technique. It was feasible to calculate the samples piezoelectric constants from the slope between the voltage change and the displacement (mV/mm). In this instance, the sample with the most zirconia particles (5 wt% MOF) had the greatest value. As seen in Figure 2.14b, these samples demonstrated a voltage peak of up to 600 mV when a force of 5N was applied, indicating improved performance in comparison to conventional pressure sensors. By taking arterial pulse measurements under typical circumstances, the electrical response of the sensor was investigated. 568mV output voltages were obtained with a sensitivity of 0.118 V/N. Its findings allowed for the deduction that the chemistry and topography of the nanofibers, in addition to the increased crystallinity of zirconia nanoparticles, influence the piezoelectric behaviour [29]

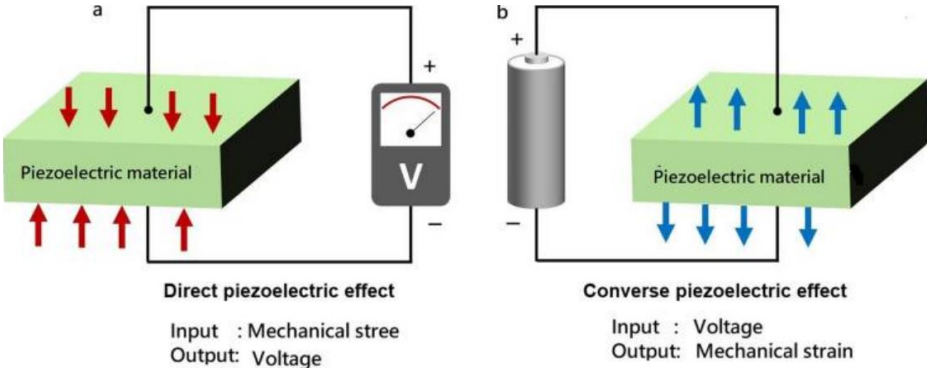

Figure 2.13. *(a) Direct piezoelectric effect applying a mechanical stimulus and (b) converse piezoelectric effect applying a voltage [30]*

Since electrostatic interactions are always present to regulate various cellular and biological functions like muscle contraction, protein folding, and bone tissue mineralization and remodelling, the piezoelectric effect has also been studied in various natural materials and human body structures [31] [32] Bone, for instance, is continuously subjected to compressive and tensile forces, to which collagen fibres react by producing an electrical charge. Specifically, the presence of hydroxyapatite and the displacement and polarisation of hydrogen bridges present in collagen crystals are thought to be responsible for the piezoelectric effect [30] This phenomenon has even been observed in certain biomolecules, such as glycine or other proteins, whose spatial configuration, chemical structure, and amino acid sequence can all alter their piezoelectric characteristics.

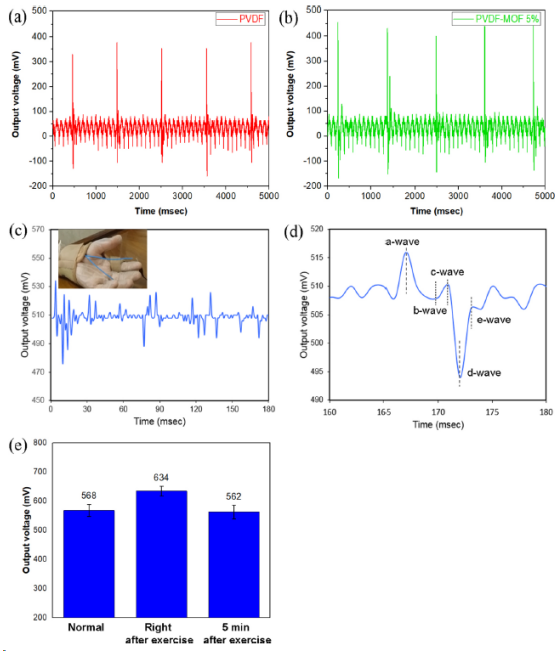

Figure 2.14. *Output voltage measured with piezoelectric sensor using a (a) PVDF and (b) PVDF-5 wt% nanofibrous membranes. (c-d) Electrical responses obtained from the pulse of an adult. (e) Monitoring under normal conditions, after 1o minutes physical activity and 5 minutes relaxing after the exercise [29]*

Lately, researchers have chosen to employ materials that are more environmentally friendly because the production of conventional sensors often produces large amounts of non-biodegradable and non-recyclable electronic waste that can be hazardous. For instance, Lu et al. designed a biodegradable and recyclable piezoelectric sensor based on bacterial cellulose (BC). Utilising molecular ferroelectric imidazolium perchlorate ($ImClO_4$) on the cellulose matrix, they were able to increase the piezoelectric capabilities and achieve a high sensitivity in comparison to other biomaterial-based sensors. This enabled for an operating range of 0.2 to 31.25 kPa. This idea has the great advantage of not producing electronic waste that might harm the environment because cellulose can be degraded into glucose and oligosaccharides while $ImClO_4$ can be recycled and used again in other devices [32]

The piezoelectric effect has been heavily utilised during the past two decades, particularly in the biomedical industry, as a result of efforts to create smart materials that can be controlled to react to external stimuli. Disease treatments, tissue regeneration, and drug delivery are a few of the more recent uses. By utilising the frequency shift that occurs when an analyte interacts with an enzyme or antibody on a material's surface, these sensors can be used to measure and examine the quantity of biological analytes in the context of diagnosing illnesses like cancer. As a result, they can be useful for the identification of target molecules or biomarkers. Due to their electromechanical conversion ability these devices can also be used for electrotherapy in different diseases. Regarding cancer, it is possible to manipulate the ionic channels and impede the growth of cancer cells by manipulating the electrical potential that a piezoelectric sensor generated by mechanical deformation. Similar to this, for the tissue engineering, these devices can be used to create potentials that control calcium channels and encourage cell differentiation for faster wound healing or bone formation using piezoelectric scaffolds [30] [33] .

2.2.4. Triboelectric sensors

Opposing charges are induced on both surfaces of two materials when they come into contact, creating a triboelectric effect that can be measured and utilised for various purposes. This phenomenon occurs when a mechanical stimulus is delivered, and the materials approach each other. Based on the triboelectric polarity difference of the materials, an electrical potential is formed between surfaces. Engineering uses these kinds of sensors extensively because of their low cost, environmental friendliness, self-powered ability, and straightforward construction [18] [34] . There are various ways these sensors can function, which are outlined below:

Contact-separation mode: It is the simplest and most fundamental method, in which an external stimulus forces two materials with dissimilar dielectric qualities to approach or separate. When two surfaces come into direct contact, an electronic affinity causes a charge to form on their surfaces. However, when they are separated, a gap forms between the layers and a potential is created in the interfacial region. This causes an electron flow between the opposing electrodes to balance the electrostatic field and make up for the potential difference (Figure 2.15a) [35] [36] . Although some arrangements are simpler to set up and have greater flexibility, their performance isn't the best.

Linear-sliding mode: These materials are stacked on top of one another to allow for sliding, when the materials move, the contact area between them changes, altering the electrostatic balance and producing a potential. An opposing charge density is produced at the point of contact, whereas electrical charges appear on the surfaces, as seen in Figure 2.15b, at the dislocated portions where the charges are not compensated [36] . Friction has the potential to compromise the sensor's longevity, which is a complication of this design.

Single-electrode mode: Unlike the configurations listed above, which employ two electrodes, this one is based on the utilization of a single electrode. While the dielectric layer is freely movable laterally and vertically, the electrode-containing layer is fixed to the ground (Figure 2.15c). Electrons flow between the electrode and the ground is caused by the moving layer's displacement, which also alters the electrostatic balance [35] [36] . It's a less complicated, adaptable, and versatile configuration.

Freestanding triboelectric-layer mode: This model is made up of a movable dielectric layer with no connections and two electrodes joined by a load. The electrodes are spaced slightly apart from the dielectric layer and are symmetrical. An induction load distribution and an electron flow between the electrodes along the load are produced by the movement of the dielectric surface [36] The model in question is shown in Figure 2.15d.

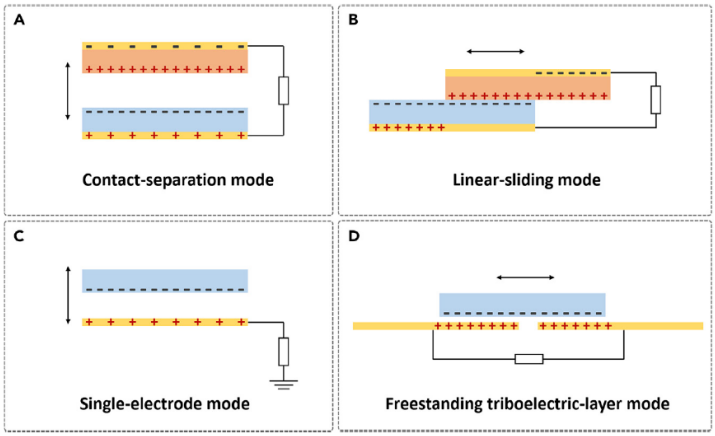

Figure 2.15. *Operating modes of triboelectric sensors: (a) Contact-separation mode, (b) Linear-sliding mode, (c) Single-electrode mode and (d) Freestanding triboelectric-layer mode [34]*

Numerous factors, including temperature, humidity, surface roughness, and movement requirements, might affect a triboelectric sensor performance. The composition of the material and its capacity to gain or lose electrons is one of the most important criteria, yet, directly manipulating this property in materials can be difficult, which is why other options are selected [21] [36] Increasing the contact area by surface functionalization or modifications is one method utilised to raise the charge density. For instance, Zhao et al. constructed a deformation sensor using poly(2-acrylamido-2-methyl-1-propanesulfonic acid) (PAMPS)-based ion gel for the triboelectric layer and electrode. In order to adjust the contact area in response to applied force, a micropatterned layer of PDMS was inserted between the layers. This allowed for quantitative control of the electrical output signals magnitude in response to deformation, enhancing sensitivity and preserving good linearity even when high voltage forces were applied [37] Reinforcements can also help to improve material properties. In their work, Hao and colleagues describe how they reinforced the dielectric layer of a triboelectric patch of graphene and polyethylene terephthalate (PET) by taking advantage of the porosity of a polyurethane sponge. To control the mechanical characteristics of the dielectric layer and enable the device to withstand high pressures, a sponge was placed in between the graphene layers. Even at high pressures (50 kPa), sensor sensitivity (0.21 kPa-1) outperformed conventional triboelectric solid layers. Additionally, a larger range of deformation limits were made possible by the porous microstructure [38] A few instances of physiological signal measurements using the patch, including pulse, blink, swallow, and respiration, are shown in Figure 2.16.

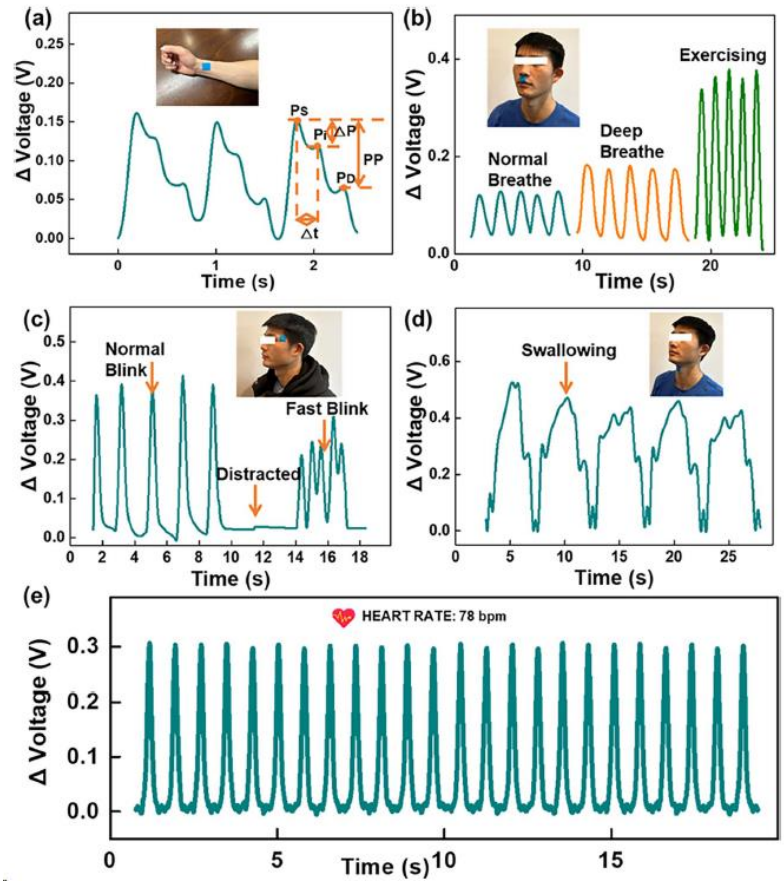

Figure 2.16. *Physiological signal monitoring of: (a) pulse wave, (b) respiratory rate, (c) blink frequency, (d) swallowing rate and (e) heart rate [38]*

Preventing the deflection and recombination of surface charges can also enhance performance by preventing alterations or decreases in the triboelectric potential. In this instance, it's imperative to prevent flaws or irregularities in the materials internal structure or surfaces [38] For instance, polymers can incorporate thin films of highly permeable metal oxides or aromatic compounds. Conventional metal electrodes are typically not the best option for triboelectric sensors since they are continuously subjected to frictional forces. Lately, sensors with a high degree of freedom and flexibility have been able to adapt to surfaces and integrate with other materials more effectively because to the development of flexible electrodes [39] [40] Conductive elastic nanocomposites, such as hydrogels, metallic liquids, or silver elastomers, are some of the materials used to construct this kind of electrodes.

2.2.5. Piezoionic sensors

One of the most recent discoveries regarding tactile sensors has been the piezoionic phenomenon. In this case, applying a deformation to the material results in the separation of cations and anions, which generates a chemical potential that can be quantified as an electrical response [41] [42] . This is a typical mechanism of deformable, soft materials like gels, which contain moving ions that can be displaced by the action of an external force (Figure 2.17) [42] . Since the free moving ions are obstructed by the hydrogels microporous and interconnected structure within the matrix, the difference between the free moving ions and the fixed chains permits a conversion of the compressed hydrogels mechanical and electrical energies [43] . Around 1990, this behaviour was first observed in polymeric compounds, however, it wasn't until 2015 that the term "piezoionic" was first used in the literature in 2015 by Sarwar and his colleagues, who developed a tactile sensor based on a polyurethane (PU) hydrogel containing different electrolytes [42] The origins of a piezoionic effect on materials are still under investigation and discussion today. One explanation for this behaviour is that it is thought to be related to a non-homogeneous ionic distribution, like the ions passing through the channels in the cell membrane that produce the Donnan's potentials [42] Once the Donnan equation is solved, it is possible to link the voltage to the ionic concentration. The equation that follows illustrates how the change in electrical potential (ΔE) must equal the change in chemical potential exerted by the external force:

$$\Delta E = \frac{RT}{zF} \ln\left(\frac{[i^+]_x}{[i^+]_{x+\Delta x}}\right) \tag{2.6}$$

Here, R stands for the gas constant, T for the absolute temperature, z for the charge valence of the ion, F for the Faraday constant and [i] denotes the concentration of i species, and its subscript denotes two sites separated by a distance Δx between the samples [42] Given that the electrical response increases linearly with the deformation as demonstrated by other research findings, it has been proposed that stress gradients, as opposed to Donnan gradients, may be the primary source of the piezoionic effect [41] [44] Consequently, it is possible to establish that the induced voltage (∇V) is directly proportional to the pressure gradient (∇P) as shown in equation 2.7 [45] .

$$\nabla V = \alpha \nabla P \tag{2.7}$$

According to Dobashi et al., the piezoionic coefficient, denoted by α, is determined by the way that moving ions diffuse through a hydrogel matrix's pores. The hydrodynamic convection force acting on these ions results in the cations and anions moving at different speeds than the solvent, which creates the potential difference. Mobility can be inferred by the diffusion coefficients of cations (D+) and anions (D-) within the hydrogel with respect to the diffusion coefficients D_{o+} and D_{o-} due to the solution, that is, without obstruction of the polymer [45] . The following equation can be used to describe the piezoionic coefficient in a porous medium using Darcy's law:

$$\alpha = -\frac{eN\kappa}{\sigma\eta}\left[\frac{D_+}{D_{o+}} + \frac{D_-}{D_{o-}}\right] \tag{2.8}$$

where, e is the electronic charge, N is the concentration, κ is the matrix permeability, σ is the ionic conductivity, and η is the fluid viscosity. There are numerous variables that affect how ions interact with the polymer. Although the hydrodynamic component that pulls ions through the pores cannot currently be measured or quantified, this coefficient is a substitute for estimating the electrical response and its behaviour [45] .

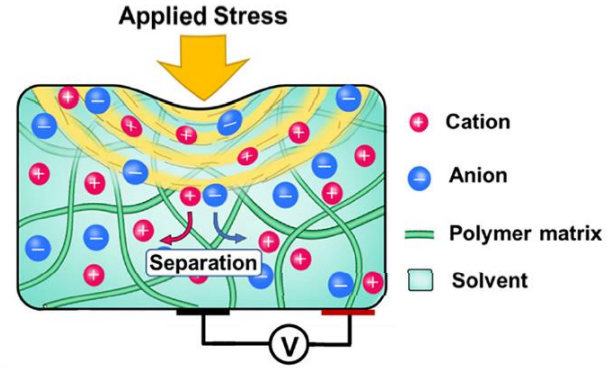

Figure 2.17. *Piezoionic transduction mechanism [41]*

Elastic pore relaxation refers to the change in the free volume of the polymer matrix that occurs when hydrogels undergo conformational deformation and a spatial distribution of ions. This process preserves the volume of the hydrogels by allowing them to reconstruct their porous structure in response to mechanical stresses [46] . Through the development of an electronic skin that can produce luminescence (ECL), Lee et al. were able to investigate visco-poroelastic behaviour in a thermoplastic polyurethane (TPU) polymer matrix embedded with an ionic transition metal complex (iTMC) and an ionic liquid (IL). Using a constant 5% deformation on several samples, load relaxation was tracked over a predetermined amount of time to analyse visco-poroelasticity. Based on their findings, which showed that the relaxation in the films containing the ionic liquid persisted over time, they concluded that visco-poroelastic deformation leads to a piezoionic effect inside the matrix that is brought on by ionic transport and stress distribution, thus, the transient stress distribution built in the visco-poroelastic TPU and the varying transport capabilities of the ionic components in the film in response to the built stress distribution are the sources of the piezoionic effect under a load [46] . By measuring the output voltage between two electrodes positioned above and below the TPU film during 10kPa cyclic compression, the researchers were able to validate their theory. The electrical response is seen in Figure 2.18, where positive and negative output voltages are visible based on the dominating valence's polarity. The voltage also reverts to its initial value after the pressure is released and a uniform distribution of ions is achieved.

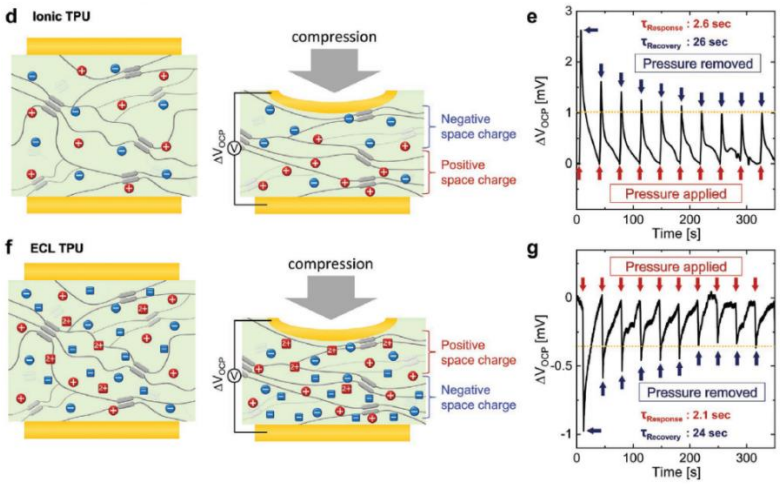

Figure 2.18. *(d) Schematic illustration of distribution of ionic components in a TPU film (left) in equilibrium and (right) under compression applied. (e) Measurement of the open circuit voltage of a TPU film under cyclic pressure (10 kPa) applied. (f) Schematic illustration of distribution of ionic components in an ECL TPU film (left) in equilibrium and (right) under compression applied. (g) Measurement of the open circuit voltage of an ECL TPU film under cyclic pressure (10 kPa) applied [46]*

Piezoionic effect-based sensors have the major benefit of requiring no external power source because transduction is entirely provided by an electrochemical process owing to ionic motion brought on by deformation. Liu et al. employed an ionic liquid containing gold (Au) and chlorine (Cl) particles as an electrolyte and a membrane of an ionic polymer metal composite (IPMC) from Nafion as a substrate to create a wearable and self-powered sensor that could track human activities. To assess various electrical signals in the body, the membrane was positioned in between two conductive electrodes [47] Figure 2.19a and Figure 2.19b, illustrate how the sensor was utilised to track wrist flexion in various directions and a seated person's posture, respectively. This sensor enabled the achievement of 1.3 mV of voltage output, a 50 ms response time, and the ability to determine the direction of the applied external stimulus.

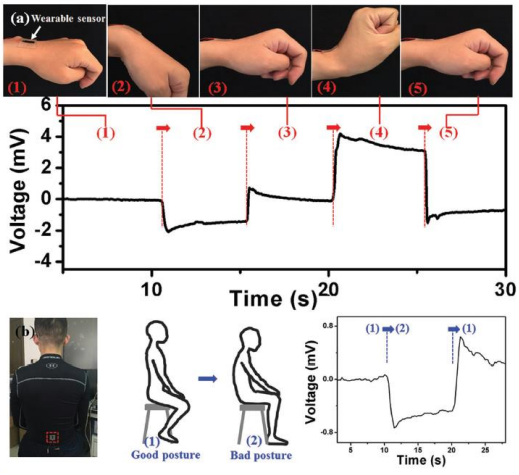

Figure 2.19. *Application of the sensor (a) to detect the flexion of the wrist in different directions and (b) monitoring the posture of a seated person [47]*

As was already established, the piezoionic effect is thought to operate by converting an external input into an ionic current, which is how humans perceive touch. Dobashi et al. designed a piezoionic skin that could reach the ranges of electrical potentials of cells and functioned similarly to skin mechanoreceptors. In order to conduct nerve stimulation on a rodent, they constructed a piezoionic sensor for the research that was made of a polyacrylamide (pAAm) hydrogel embedded with sodium chloride (NaCl) and attached to the mouse's tibial nerves via needle electrodes (Figure 2.20a). An electromyogram was also recorded by connecting electrodes to the gastrocnemius muscle [45] After assembly, the sensor was pressed, and it was possible to notice an electromyograph signal (EMG) during muscle activation by the induced current pulses generated by the sensor. The EMG results are presented in Figure 2.20b.

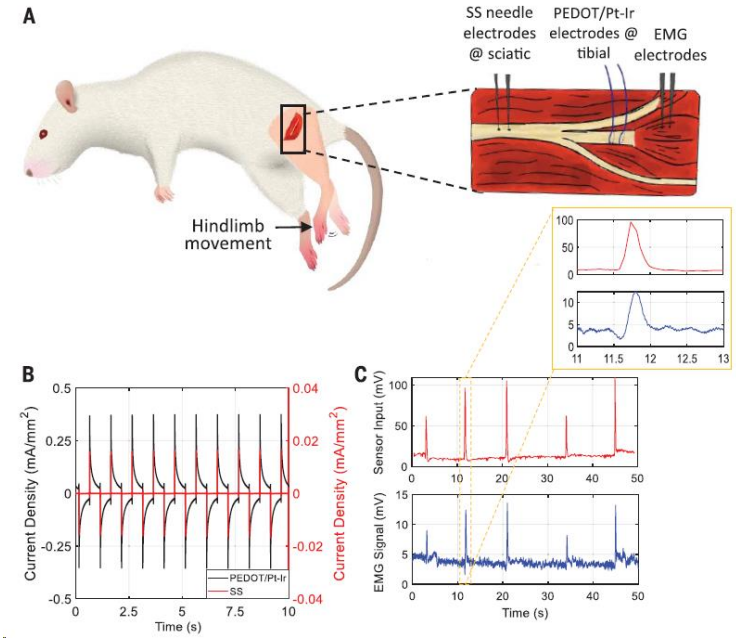

Figure 2.20. (a) *Set up of the location of electrodes connected to the piezoionic sensor for nerve stimulation in the rodent*. (b) Current responses to a square wave. (c) *Sensor voltage and EMG signal reading during piezoionic stimulation [45]*

Despite being relatively new and understudied, the piezoionic effect can be a fantastic substitute for the above-mentioned standard techniques These sensors provide excellent performance and versatility in a variety of environments because to their self-power capability. Moreover, because of their mode of operation and high degree of biocompatibility, they facilitate the development of novel medical devices and allow for good integration with biological systems [41] In addition, they can be useful for the detection of complex movements that are multidirectional, taking advantage of the sense of the electrical potentials they produce [47] . While more research is required to fully understand this occurrence, these devices have the potential to enhance the functionality of future tactile sensors.

2.3. Hydrogels

Hydrogels are polymers characterized by an interconnected three-dimensional network and a high water content. They have a remarkable ability to absorb water and expand its volume without losing its shape, and their constitution permits them to be soft, deformable materials with elastic and conductive capabilities [48] [49] Hydrogels can be categorised using a range of criteria, as seen in Figure 2.21, due to the multitude of attributes and variables that may influence their behaviour. These can have synthetic or natural origins. Natural hydrogels are made mostly of polysaccharides and proteins, some of which include cellulose, chitosan, collagen, hyaluronate acid, and gelatine. They originate from a wide range of environmental sources. Due to their structural and functional similarities to the soft tissues of the body, these materials are highly appealing in the medical field. They also have limited mechanical qualities and stability, but they are also very biocompatible, biodegradable, and bioactive. In contrast, those with a synthetic origin are made by polymerizing monomers like polyvinyl alcohol (PVA), polyethylene glycol (PEG), polyethylene oxide (PEO), polyacrylic acid (PAA), or polyacrylamide (PAAM) [50] As they are artificial polymers, their mechanical properties can be adjusted or manipulated, they are more stable, but are not as biocompatible and biodegradable. In some cases they can be hazardous for the human body. Table 2.1 shows the main advantages and disadvantages of synthetic and natural hydrogels.

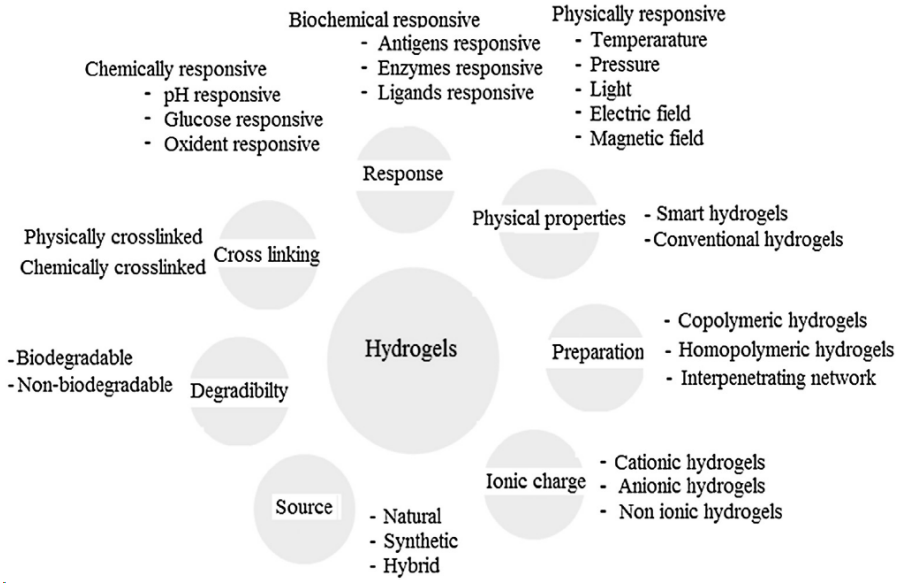

Figure 2.21. *Classifications of hydrogels according to different criteria [51]*

To give a define shape to the hydrogel, physical or chemical crosslinkings are used to create bondings between the polymer chains. Chemical crosslinking is based on covalent interactions that result in long-lasting configurational changes in the hydrogel, whereas physical crosslinking is achieved by techniques based on non-covalent interactions like electrostatic and hydrophobic interactions or hydrogen bridges, which can be reversible [51] [52]

	Natural hydrogels	Synthetic hydrogels
Advantages	• Nontoxic • Biocompatible • Biodegradable • Promote cells adhesion • Promote cells growth • Promote cells proliferation • Promote cells differentiation • Promote cells ECM secretion	• Controllable microstructure • Controllable degradation • Long shelf life • Tailored functionality • Strong mechanical properties • Wide varieties of raw chemical resources
Disadvantages	• Low mechanical strength • Batch variation • Risk of disease transmission (ECM-based hydrogel)	• Low biocompatibility • Risk of inflammatory response • Risk of immunological response

Table 2.1. *Advantages and disadvantages of natural and synthetic hydrogels [53] .*

According to their constitution and preparation methods, hydrogels can be classified as homopolymers when they are made from a single species of monomer and copolymers when they are composed of two or more types of monomers in the same polymer chain. Copolymers can vary depending on the order of their monomers within a polymer chain (Figure 2.22). In addition, hydrogels can have two or more different kinds of polymer chains and have semi-interpenetrated (semi-IPN) or interpenetrated (IPN) networks. While interpenetrates hydrogels are made up of two or more polymers that are crosslinked in the presence of a chemical agent, semi-interpenetrate ones are linear polymers that penetrate another network without the need for further chemical agents [50] [51] . Figure 2.22 shows the many kinds of hydrogels that were previously discussed.

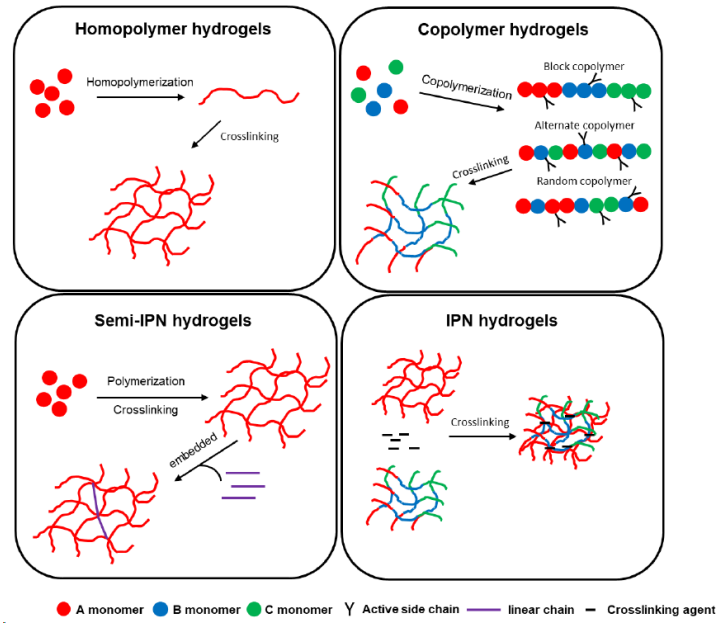

Figure 2.22. *Illustration of a homopolymers, copolymers, semi-IPN and IPN hydrogels [50]*

Another characteristic from these materials is that when they are exposed to water or a suitable solvent, hydrogel can swell. The polymer chains relax by hydration and the system

expands as the liquid starts to permeate the structure and diffuse its molecules throughout the matrix. The balance between the osmotic pressure and the elastic forces that keep the structure from deforming is known as the equilibrium water content, and it relates to the maximum amount of water that hydrogels can absorb [52] [54] This is a capacity that can be affected by different parameters such as the nature of the hydrogel, the crosslinking degree, or the number of functional groups in the polymeric chain [54] One challenge with hydrogel absorption is that water can evaporate at high temperatures, dehydrate in dry environments, or freeze below 0°. In these situations, mechanical deformability and stable electrical properties cannot be maintained in extreme situations [49] [52] .

These materials can react to a wide range of external stimuli, including changes in pH, light, temperature, force, or the presence of molecules. Hydrogels have a volume-phase shift or transition in response to environmental stimuli because of several molecular interactions that may alter their network. These modifications may manifest as adjustments to the materials properties, or as modifications to its dimensions and shape [52] [54] . A clear example was the system designed by Zhang and his colleagues, which employed an injectable hydrogel comprising chitosan (CS), hyaluronic acid (HA) and sodium glycerophosphate (GP) that could react to pH and temperature variations to release a drug locally to treat cancer cells. To make the hydrogel, 1 mg of the anticancer medication doxorubicin (DOX) was added to the base solution. The carboxylic groups in hyaluronic acid can react and build hydrogen bridges with the amino groups in chitosan, which can mechanically reinforce the hydrogel and reduce the drug's burst release. The hydrogel is prepared and kept in a liquid state at 4°C and once injected it is transformed to a gel state by the increase in temperature within the body (37°C). Since it is injected, hazardous effects in other body sections where cancer cells are absent are minimised and a localised release from the pharmacy is made possible. The acidic environment of the tumour promotes the drug's release [55] . Figure 2.23a presents the results of the release of the drug over time at different pH values in samples with different HA contents. When the pH is more acidic (pH=4.00) there is a greater release of the drug, likewise, the percentage of accumulative release increases gradually with the HA content. Figure 2.23b and Figure 2.23c illustrates the drug release data after 130 hours at pH 4.00 and pH 6.86, respectively.

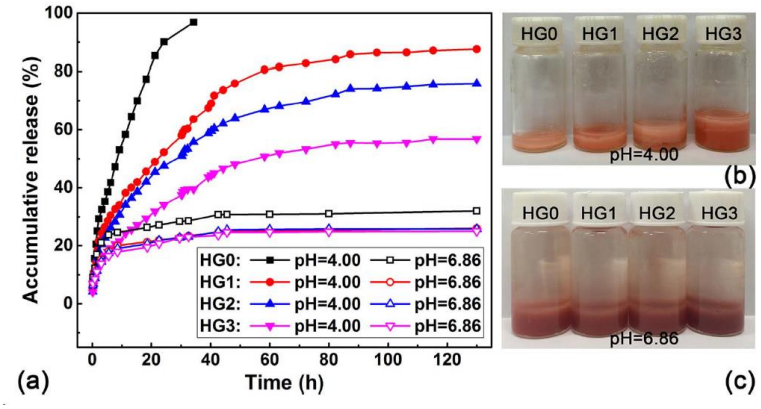

Figure 2.23. *(a) Results of the accumulative release of DOX at different pH values using samples with different HA contents. Pictures of hydrogels after 130 hours the release of drug at (b) pH 4.00 and (c) pH 6.86 [55]*

Hydrogels are materials that have stood out for their versatility and tuneable mechanical properties. The range of applications in which they can be used is increased by their ability to be moulded into precise sizes and forms, which allows them to be miniaturised and incorporated into systems at small scales. Furthermore, these devices can function as active sensors or be included into the structure of a sensor [52] They are currently being employed extensively to bridge the gap between robust artificial machines and soft biological systems by utilising their transparency, elasticity, ionic conductivity, flexibility, and biocompatibility [49] Enhancing hydrogel conductivity has been the focus of scientific research for the development of novel touch sensors. There is a family of polymers that are inherently electroconductive thanks to their spatial configuration containing extensive π-bonds. Electroconductive hydrogels (HEs) result from the combination of an active conductive polymer with a highly hydrated hydrogel that serves as a base. In addition to its matrix function, the hydrogel offers biocompatibility, flexibility, swelling, and the ability for molecules to move through the network [56] Among these polymers are polypyrrole (PPy), polyaniline (PAn), polythiophene (PTh) and poly(phenylene) vinylene. Because of its great conductivity qualities, PPy polymer has been widely used in the construction of sensors, electronic prostheses, artificial muscles, load cells, and actuators, however, tends to be fragile and insoluble. The combination of PPy and a well-hydrated network of poly(2-hydroxyethyl methacrylate) p(HEMA) was described by Brahim et al. as a way to create stable biosensors that might support various clinical evaluations [57] In 2010, Tsai et al. developed an electroconductive hydrogel that could perform a controlled release of a drug through sensitive erosion and electrostimulation, based on PVA and PAn as electro-active polymer [58] The cardiac patch, created by Liang and associates in 2018, is another illustration of the application of electroconductive hydrogels in the treatment of myocardial infections. In their investigation, scientists simultaneously covalently polymerized dopamine and PPy in situ using gelatine to create a conductive, stable network that was sticky and able to be held together on the surface of the heart preventing liquid filtration. Based on their findings, a therapeutic patch was created that enhanced cardiac function in heart failure, myocardial revascularization, and the production of electrical signals (Figure 2.24) [59] [60]

Electrolytes are substances that contain free ions and can be employed to increase a material's conductive properties. These can be dissolved in aqueous solutions and incorporated into the hydrogel matrix. Salts such as sodium chloride (NaCl), lithium chloride (LiCl) or potassium chloride (KCl) are typically used to form electrolyte-based conductive hydrogels [2]. For example, it is possible to create portable and wearable energy storage devices using polyacrylamide (PAAm) films that are synthesized with LiCl inside. These membranes are placed between two carbon nanotube-based film electrodes to form a supercapacitor with high capacitance and long discharge time [61] Since the charge of the groups in the polymer chain's backbone only permits the passage of ions with opposing charges, electrolytes can also be organised in groups within the repeating units of polymers (polyelectrolytes) to produce selective conductivity [2]. The main issue with adding electrolytes to hydrogels is that sometimes they are not biocompatible and can be found in high quantities. This means that electrolyte leakage from the hydrogel into bodily fluids can occur, which can have an impact on the body's water balance and metabolism. Some of the most common polyelectrolytes are polypeptides, glycosaminoglycans, DNAs, poly

(diallyldimethylammonium chloride) (PDAC), poly (sodium styrene sulfonate) (PSS), and polyacrylic acid (PAA) [2].

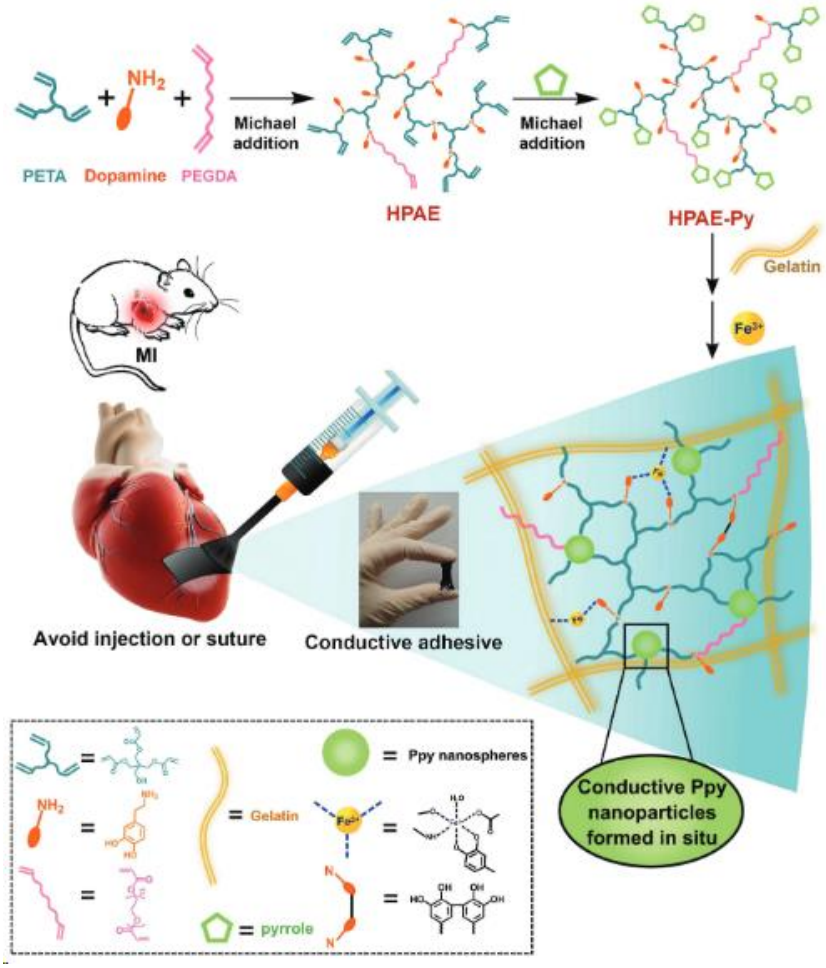

Figure 2.24. *Schematic of the development of a conductive and adhesive hydrogel and its application as a therapeutic patch for heart failure [59]*

Using ionic liquids (LI), which are hydrolytically stable fluids made of inorganic anions and organic cations with melting temperatures below 100°C, is one of the most innovative approaches to creating conductive hydrogels. These are materials that, at both high and low temperatures, do not evaporate or crystallise [2] [62] Ionogels are created by synthesising ionic liquids inside ionic polymers using chemical or physical crosslinks to create a three-dimensional structure. They are often quite stiff compounds with low tenacity, and they are only soluble in polar organic solvents. Cao et al. succeeded in creating a transparent ionogel with good mechanical properties and high stability by creating a bonding hydrogen between poly(ethyl acrylate)-based (PEA) elastomers and 1-ethyl-3-methylimidazolium bis-(trifluoromethylsulfonyl)imide ($[C_2mim][NTf_2]$) ionic liquid. The system mechanical and electrical properties could be controlled based on the degree of crosslinking and LI content. The ionogel exhibits high elasticity between 15 and 484 kPa, durability up to 10,000 cycles at 100% deformation, and deformability up to 5000%. Following material characterization, the

material was used as a sensor to track various movements even in harsh environments like high vacuum, extreme temperatures, and high humidity [63] Several of the findings from the study are shown in Figure 2.25.

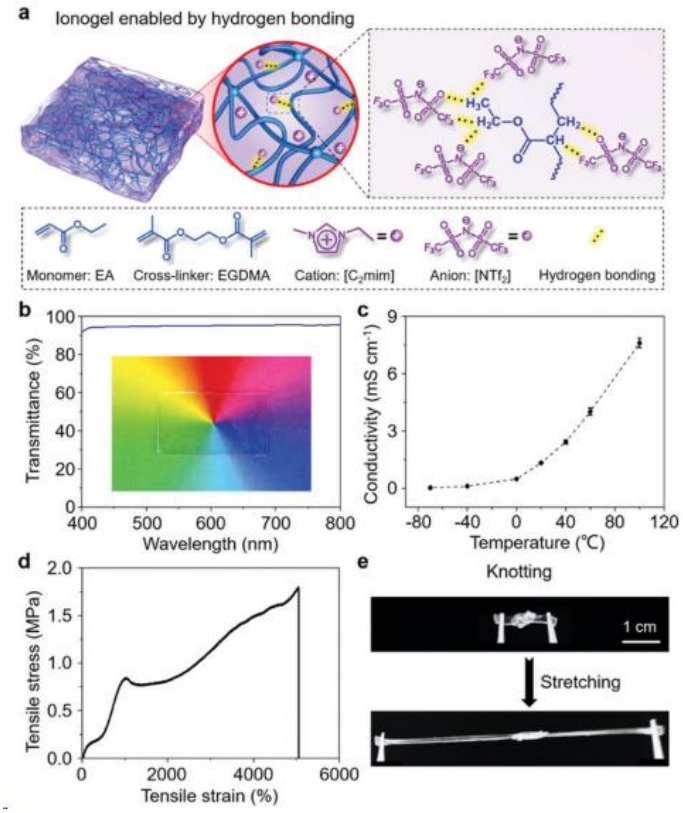

Figure 2.25. *(a) Schematic of the ionogel formation using hydrogen bonding with the PEA matrix. (b) Transmittance in the visible range (wavelength, 400–800 nm) of ionogel film. (c) Graphic of ionic conductivity versus testing temperature. (d) Tensile stress–strain curve of the ionogel. (e) Images of the ionogel under a mechanical deformation [63]*

2.4. Tactile sensors applications

As was already mentioned, tactile sensors are devices that may provide electrical responses when mechanically stimulated by physical touch [22] The need to develop new materials that meet these requirements and enable safe human-machine interaction has arisen because conventional sensors today face a variety of challenges, including achieving high resolution and sensitivity, reducing environmental impact and high energy consumption, good stability, and adhesion on various surfaces [2]. Lately, tactile sensors have become an essential part of the most innovative, advanced, and intelligent systems that allow high recognition and interaction with the environment [21]. The development of extremely flexible and deformable sensors, which are inspired by the sensory functions of human skin, has also revolutionised the field of wearable sensing devices. Research on these sensors has led to a wide range of applications in the development of electronic skins, personal health monitoring devices, and other related fields.

2.4.1. Soft robotics

Robots are autonomous artificial electromechanical devices designed to do a wide range of human tasks fast and in large quantities. They are used to minimise the need for human intervention and effort. These devices are typically made of substantial, weighty and robust components. Increased complexity and range of motion in these systems generally exacerbate other problems, like having a significant impact on the environment, becoming more unstable. Moreover, they are challenging to integrate with humans and adapt to different surfaces [64] In consequence, a gap has been created between human interfaces and machines. As a result, it is now necessary to develop a new generation of soft robots, which call for smart materials that are malleable and extremely flexible. The research and development of touch sensors with high perceptual capacities that may be used and positioned on many surfaces has expanded in an effort to enhance these systems [2]. The soft tissues and biological systems of the human body serve as an inspiration for soft robots. Since they can adapt to a wide range of deformations, they are typically made of materials like silicones or elastomers. Ionic hydrogels are also frequently utilised in this field [65] For example, to investigate marine life at the ocean's bottom, Phillips et al., created a robotic arm with several degrees of freedom. Through the use of an integrated glove with soft rubber Ecoflex sensors, the system may be operated remotely. These sensors enable the control and synchronisation of valves that apply pressure to the robotic arm and soft actuators. Some photos of the robotic system are included in Figure 2.26. With its minimal power requirements, the arm can reach depths of more than 2300 metres [66]

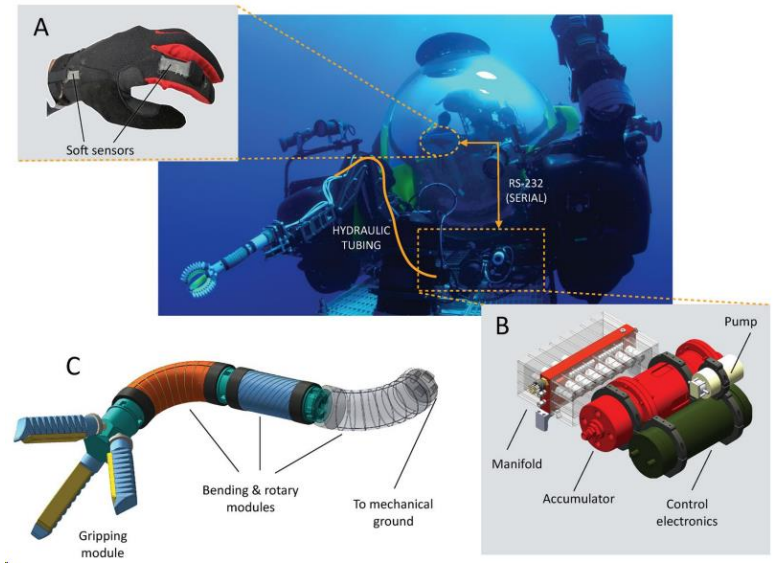

Figure 2.26. *Deep-sea soft robotic arm components. (a) Soft sensorized wireless glove. (b) Illustration of the control open-circuit seawater engine. (c) Schematic of the soft robotic arm [66]*

Soft robots have a well-integrated design and do not require a complete assembly, in contrast to standard rigid systems that must be built. Instead, they can be compacted in a single process or by a simple adhesion of their pieces. Rapid prototyping methods like 3D printing have been very helpful in the development of intelligent systems. With this

approach, devices can be constructed more quickly, directly, and with complicated architectures while using less material. Furthermore, conductive or dielectric materials can be deposited more easily and in fewer steps, and multi-material depositions can be created [67]. A 3D printed hand with tactile sensors integrated into the phalanges to enable an inherent soft capacitive touch is presented in Figure 2.27, along with the production process.

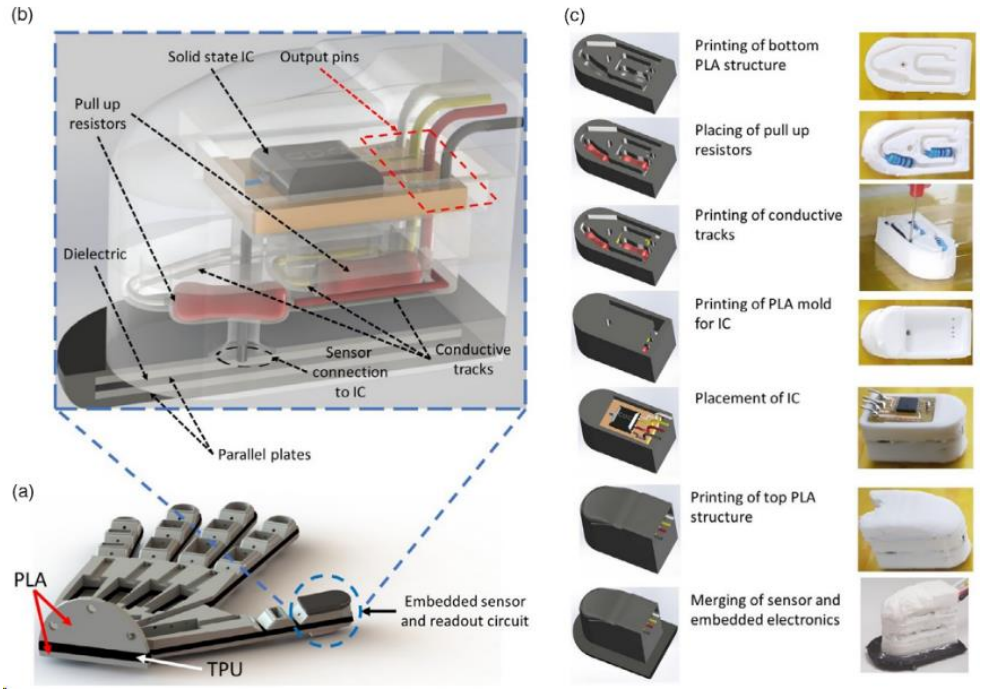

Figure 2.27. *(a) CAD design of the Ecoflex hand with the smart sensing phalanx. b) CAD design of the interior structure of the phalanx. c) Fabrication process for the 3D printed hand [68]*

2.4.2. Electronic skins

Distinctive and well-organized structures both within and outside the skin serve as the primary basis for tactile sense. The sense of touch is disrupted when these structures are lacking due to diseases or alterations. Electronic skins, or e-skin, use tactile sensors that can translate external stimulus into electrical signals to replicate the biological behaviour of the skin and its information-transmission system [69] In order to be incorporated on various surfaces, integrated into clothing or in contact with human skin, biocompatible, flexible, light and deformable materials are used [70] . One of the most popular methods for creating artificial skins is the combination of flexible plastic substrates and embedded with an active material. To increase their flexibility and lessen pressures on the active material, the substrates dimensions might be lowered, making them thinner and narrower. Polyurethanes, silicone, PDMS, and Ecoflex are a few materials that are employed [71] . Using a pre-deformed elastomer as a substrate is one method of creating flexible electronics, this is known as buckling, and occurs when the flexible membrane exits the deformation plane, and its stretch deforms the active element. Discontinuous patterns of stiff components on a deformable substrate are an additional option, in this case, deformation is dependent on the spaces between the hard pieces that can be deformed. Additionally,

composite, or modified materials that are naturally stretchable can be used as well (Figure 2.28) [72] .

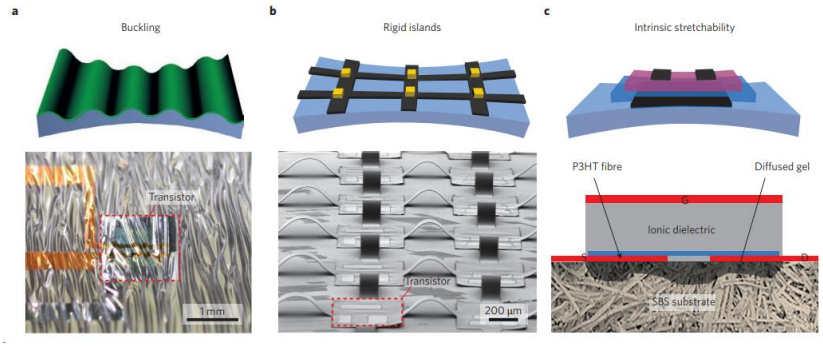

Figure 2.28. *Various ways to implement flexible substrates to form tactile sensors used in electronic skins: (a) Buckling, (b) Rigid islands and (c) Intrinsic stretchability [72] .*

On a broader scale, tactile sensors can also be used to cover bigger surfaces, an electronic skin, for instance, could be designed to cover a whole hand prosthesis. In this case, active-matrix arrays are employed with very thin and soft films containing high-performance pressure sensors to achieve high spatial resolutions and faster responses [73] . Lou et al. first designed a single sensor based on polyaniline hollow nanospheres composite films (PANI-HNSCF) for their study. This hierarchical hollow design offered a major flexibility and elasticity. The film was arranged between two ultra-thin layers of PDMS with gold electrodes. A system of large-scale resistive tactile sensors (10x10 pixels) was created utilising lithography technology to mimic the sense of human touch once the sensor's characterisation and functionality were confirmed. The design was adhered to diverse hand regions and adjusted to the contours of the skin even in cases of skin deformity (Figure 2.29b). Similarly, when various items were put on the e-skin, it was possible to identify the contact between the e-skin and the objects, even if they had varied weights [74]. The pressure distribution maps of an aluminium doughnut and a human hand exerting pressure to the e-skin are depicted in Figure 2.29c and Figure 2.29d, respectively. The contact regions may be easily identified by the change of pixel colours in the matrix.

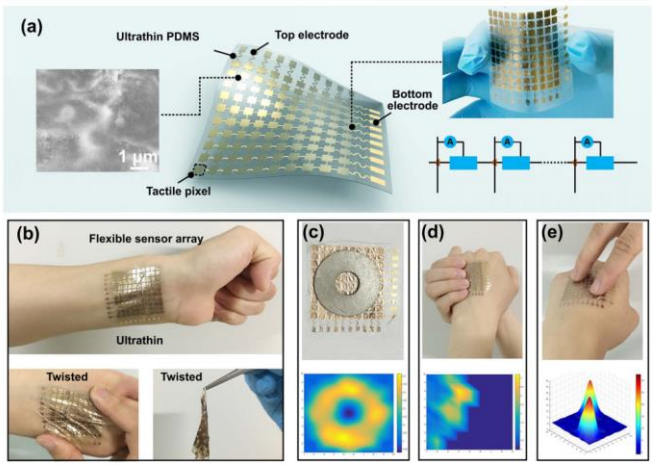

Figure 2.29. *(a) Illustration of an ultrathin and flexible sensor array with 10×10 pixels. (b) Photography of a wearable ultrathin e-skin sensor array on wrist and under a twisted deformation. (c) Metallic ring placed on the surface of ultrathin e-skin sensor array (top) and its respective pressure mapping profile (bottom). (d) An adult man hand press (top) and its respective pressure mapping profile (bottom). (e) Pressure with fingers on the array (top) and its respective pressure mapping profile (bottom) [74].*

Lu et al. created a lightweight, flexible skin sensor with great sensitivity by utilising the piezoionic effect. The device consists of a robust interface between an electrode and an electrolyte. A precursor that was seeded inside a polymeric electrolyte and inseminated with metal ions was utilised to generate the interface. The entire polymer surface is covered with a layer of metal electrode created by an ion reduction process. A strong coupling structure is formed between the metal and the polymer, while the ions are maintained near the surface of the polyelectrolyte. The cations and anions of the polyelectrolyte migrate to the deformed zone when pressure is applied to the sensor, creating an ionic concentration gradient that can be converted into an electrical output [75] . The sensor was used in certain practical applications to identify tiny electrophysiological signals from human skin, including eye blinking (Figure 2.30b), facial expressions created while puffing up the cheek (bulging) (Figure 2.30c), and finger movements (Figure 2.30d). For the measurements, just half of the sensor construction was utilised.

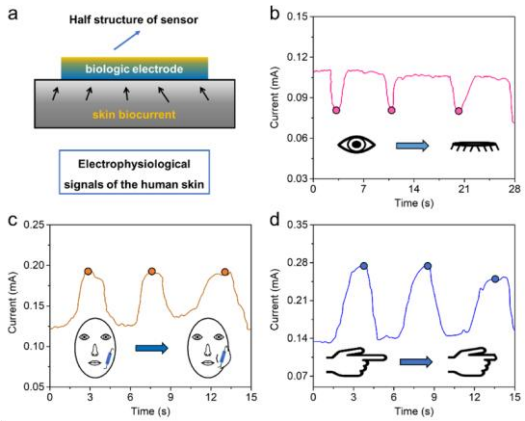

Figure 2.30. *(a) Half structure of the piezoionic strain sensors for detecting electrophysiological signals of human skin. (b) Current signal response of eye movements. (c) Current signal response for monitoring cheek bulging. (d) Current signal response of finger movements [75] .*

Owing to their capabilities and most recent advances, e-skin has demonstrated excellent implementation in a variety of applications, including robotics, health monitoring, and artificial prosthesis [72] . Recently, there has been a push to use artificial intelligence and deep learning techniques to synthesise the processing of tactile input and apply the sensory arrangements that compose the e-skin to reach a new level of development that may involve the skin's natural sensorineural behaviour in a more detailed way [76] .

2.4.3. Human motion detection

As some previous examples have shown, technical advancements and the miniaturisation of electronic components have made it feasible to track a variety of human activities, such as sports, health monitoring, and other leisure pursuits [77] . Tactile sensors in this field need to have a high degree of flexibility and deformation capacity as well as the ability to stick to surfaces that move and are subjected to different environments, such as sweaty or wet skin, in addition, they should also have the right size so that they do not interrupt the movements of the body. Acquiring real-time information of various movements (angular or linear) without being impacted by noise or crosstalk represents another difficulty for these sensors.

An innovative approach has been the development of textiles as smart materials to build soft sensors. These materials are low-cost, lightweight, flexible, easy to process and have a high adaptability. There are fibres that are intrinsically conductive, or their electrical properties can be enhanced through functionalization with conductive polymers to carbon materials [78] . Wu and colleagues, for instance, developed a highly sensitive strain sensor using a conductive polymer combination. Using a polyurethane yarn and the layer-by-layer (LbL) technique, the sensor was constructed and subsequently inserted in a PDMS matrix. The device was able to recognize a person's sob and laughing expressions [79] . Zhang et al. used graphene fibres to develop a wearable sensor capable of monitoring human movements during physical activity. They employed tiny graphene sheets and helical polyester (PE) fibres to round an elastic PU core. Figure 2.31 illustrates how the knee, ankle, and elbow movements were recorded while shooting a soccer ball. The wider and more pronounced knee and ankle motions are more noticeable in the graphs when there is a shift in resistance, in this case, when the subject is forced to hit the ball (phases B to C) [80] .

The use of tactile sensors in healthcare extends beyond basic monitoring, reaching into the realm of diagnostics. By incorporating polymer-based sensors into medical devices, healthcare providers can gather more detailed data related to touch, pressure, and movement. This information can be valuable in assessing neurological conditions, musculoskeletal disorders, and rehabilitation progress, providing a more holistic understanding of a patient's health. These smart materials can be designed to conform seamlessly to the human body, providing a comfortable and non-intrusive means of continuous monitoring, however, there is a lot of promise for integrating touch sensors with polymers, issues like standardisation, data security, and power economy must be resolved.

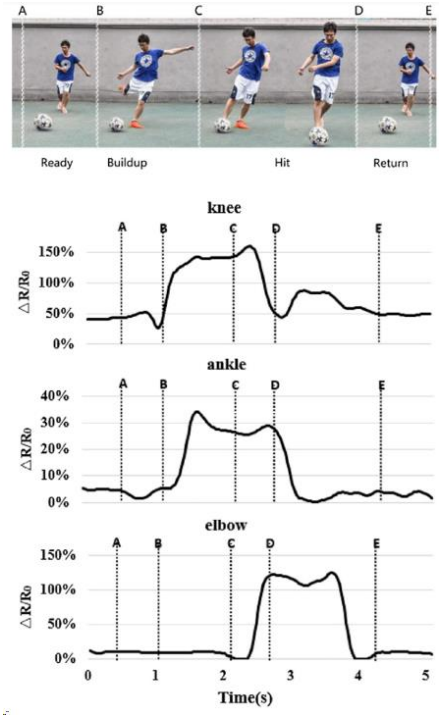

Figure 2.31. *Phases of soccer kicking motions and signals response of the wearable sensors on the knee, ankle, and elbow for the entire kicking process [80]*

On the other hand, lately, the data obtained from the tactile sensors can be linked to computational tools (Artificial intelligence and Internet of Things) to track various human activities in real time, allowing a more precise and focused monitoring in order to improve patient rehabilitation processes, personalised medicine, and disease prevention.

2.4.4. Energy harvesting

One innovative promising development involves integrating energy harvesting capabilities into tactile sensors. Traditionally, tactile sensors were primarily focused on providing feedback or information about the physical interaction with objects. However, with the growing need for sustainable and self-sufficient devices, researchers have explored ways to convert the mechanical energy generated during touch or pressure stimulation into usable electrical power. For instance, integrating energy harvesting into tactile sensors in prosthetic limbs can enhance their energy efficiency. The sensors can capture the mechanical energy produced during movement or contact with surfaces, contributing to prolonged battery life and increasing the overall usability of the prosthetic device. In the case of wearable devices, sensors can generate electricity from the user's movements or interactions with the environment, reducing the need for frequent recharging or battery replacements [81].

Triboelectric nanogenerators (TENGs) have emerged as an innovative technology at the forefront of the energy harvesting field. Their unique ability to convert mechanical energy into electrical power, based in the triboelectric effect, has not only impulsed advancements in sustainable energy solutions but has also found applications in tactile sensors. This

integration marks a significant advance in the development of self-powered, responsive technologies [82] . As an example, Liu et al. used a sandwich configuration of a single-electrode mode with copper (Cu) traces between two ultrathin layers of soft PDMS to create a flexible TENG. The device was able to sense specific mechanical stress with high selectivity and sensitivity [83] . As it shows in Figure 31, the sensor was put on the skin and various efforts were applied including touching, poking, tapping and hitting. To validate energy harvesting, the sensor was integrated with an insole to electrical responses during a walk. High voltage and current values demonstrated its high capacity to charge a capacitor (Figure 2.32) [83] .

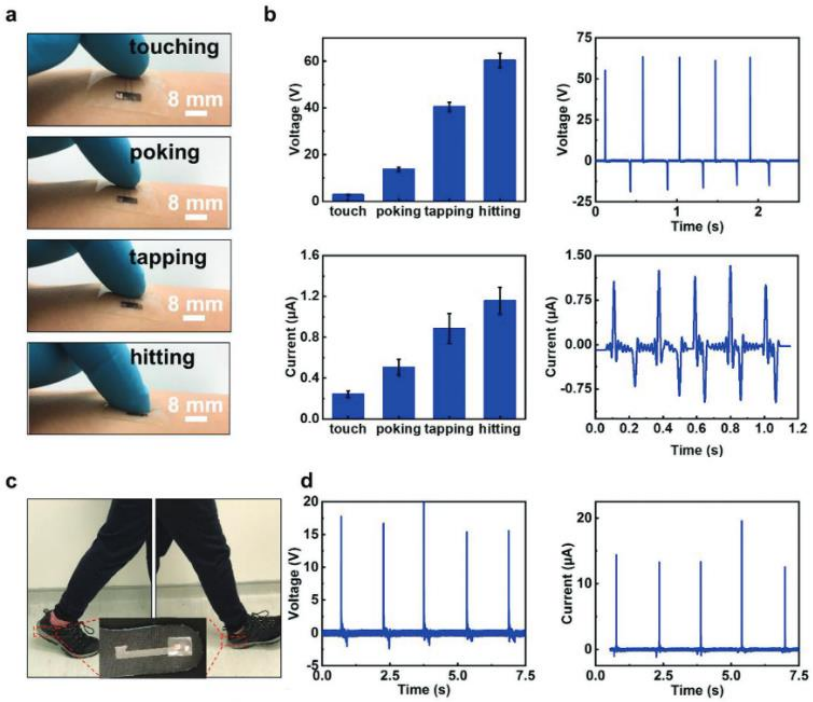

Figure 2.32. *Output signals of the TENG under different forces. a) Images of four different external forces on the nanogenerator dispose on the surface of human arm, touching, poking, tapping, and hitting. b) Voltage and current responses during force application on the TENG. c) Image of human walking as nanogenerator was attached onto insole. d) Electrical response of TENG to human walking [83] .*

Despite the promising advancements, challenges such as the efficiency of energy conversion, durability of materials, and integration into compact designs remain areas of active research. Future developments may involve the exploration of new materials, improved manufacturing processes, and innovative sensor designs to enhance energy harvesting efficiency and to increase the range of applications. In conclusion, the integration of energy harvesting capabilities into tactile sensors represents an important pathway towards creating more sustainable and self-sufficient technologies. As these advancements continue, the potential for tactile sensors to contribute and help to the development of environmentally friendly and energy-efficient devices across different industries becomes increasingly evident.

Chapter 3.

Materials and methods

3.1. Hydrogel composition

This investigation was conducted using a semi-IPN hydrogel based on Poly (vinyl alcohol) (PVA), acrylic acid (AAc) and Poly (ethylene glycol) diacrylate (PEGDA). The hydrogel is characterized by being photocurable and having self-healing capabilities. PVA is a linear polymer containing hydroxyl groups that can build hydrogen bridges with the carboxylic groups of AAc to maintain the stable structure, while PEGDA serves as a cross-linker. These substances interact through dispersion forces. The chemical covalent network acrylate precursors are added to an aqueous solution including PVA to generate the ink. UV light irradiation is then used to form the gel, homogeneously embedding the polymer within the crosslinked acrylic matrix. The gel structure can be recovered from deformation through the reversible physical crosslinkings provided by the semi-IPN network (Figure 3.1**Figure 3.1.** (a) Chemical structures of the initiator (TPO), monomer (PVA), cross-linker (PEGDA), and mending agent in the photocurable resin (AAc) [84].). As photoinitiator, diphenyl (2,4,6-trimethylbenzoyl)phosphine oxide (TPO) is used, which is compatible with water and additionally, an organic water-soluble dyes is added to improve the printing resolution [84] .

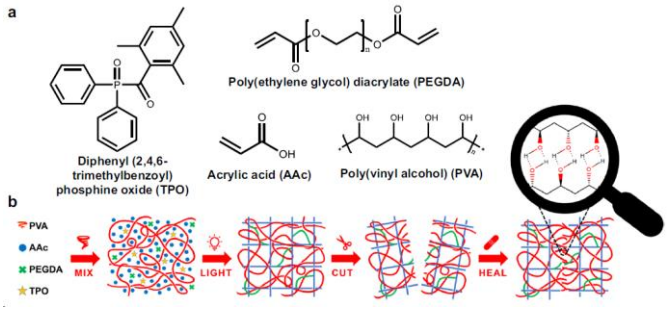

Figure 3.1. *(a) Chemical structures of the initiator (TPO), monomer (PVA), cross-linker (PEGDA), and mending agent in the photocurable resin (AAc) [84].*

Table 3.1 shows the percentages by weight (wt%) of each of the compounds used to obtain a hydrogel formulation at a concentration of 1 molar (1M).

Chemical compound	Weight (wt%)
Distilled water (H_2O)	63.68
PVA	15.92
AAc	19.90
PEGDA 575	0.20
TPO SDS	0.30
dye	0.006

Table 3.1. *Composition of the self-healing hydrogel at a concentration of 1M.*

Several salts were utilised to examine the piezoionic effect and improve the hydrogel's conductive qualities. As the least electronegative electrolytes in the periodic table, alkaline metals belong to group 1(a) of the elements of periodic table and have a single easily given electron in their valence layer, which makes them highly reactive and conductive. They react with halogens to generate salts that are very soluble in water. In this work, the cations were substituted with different alkali metals, but the anion (Cl) of each fixed salt was preserved. The salts used to investigate ionic mobility and the electrical properties of the sensor are presented in Table 3.2 with their respective atomic weights and radius.

Salt	Molecular weight (g/mol)
Lithium chloride (LiCl)	42.394
Sodium chloride (NaCl)	58.442
Potassium chloride (KCl)	74.551
Rubidium chloride (RuCl)	120.921

Table 3.2. *Chloride salts used during the research with their respective molecular weight.*

3.1. Formulation preparation

The formulation was prepared by first dissolving the required amount of salt in a container to achieve a concentration of 1M in relation to 16mL of deionized water. After that, the container was submerged in an ice-filled recipient (4°C) and stirred magnetically for 15 minutes at 150 rpm. While the system was at 4°C, 4g of PVA were dissolved within the solution (Figure 3.2a). The ice melted and the temperature rose to room temperature during the next 30 minutes of agitation. Then, the container was placed in a heated silicone oil bath at 90°C for 60 minutes while being stirred at 100 rpm (Figure 3.2b). Subsequently, the mixture was allowed to cool between 50°C and 60°C until it became reasonably homogenous. Afterwards, PEGDA (50 mg), AAc (5 g), TPO (75 mg) and dye (1.5 mg) were added to the solution. Finally, the whole solution was mixed through centrifugation at 2000 rpm for 5 minutes. The process was repeated for each of the salts.

a) 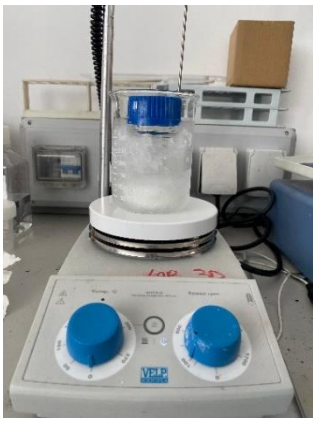

b) 

Figure 3.2. *(a) Container with formulation at 4°C under magnetic stirring at 150 rpm for 30 min. (b) Formulation inside the hot silicone oil bath (90°C) under magnetic stirring at 100rpm for 60 min.*

Figure 3.3 illustrates a step-by-step diagram of the above procedure for making the hydrogel formulation.

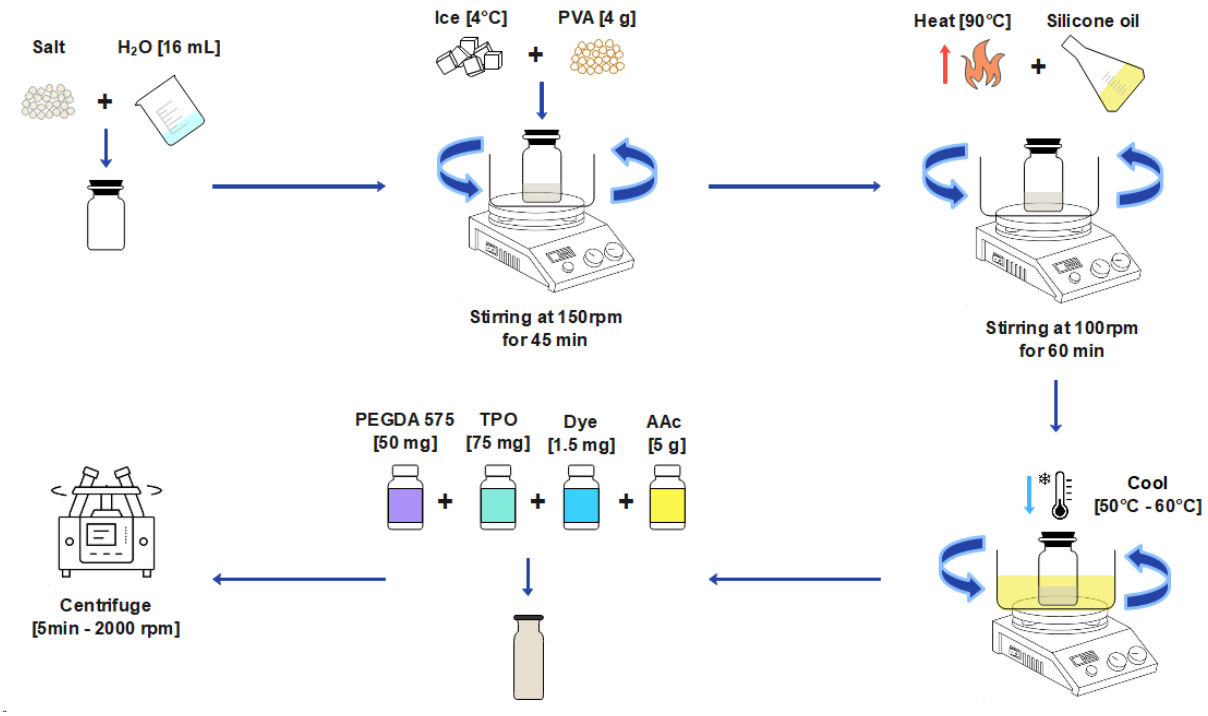

Figure 3.3. *Schematic of the method for the preparation of the hydrogel formulation.*

3.2. Sensor designs and construction

In order to run tests with different parameters, various configurations that matched the features of the machines were designed. Kapton-copper electrodes were employed to construct the sensors and the hydrogel was cross-linked into PDMS transparent moulds of different dimensions and shapes. The first model, shown in Figure 3.4a, was executed in a parallel arrangement, using the hydrogel as an elongated rectangular band (1 mm thick), to which two electrodes were affixed at the extreme sides, spaced apart by 1 cm. Conversely, a smaller version of the previously described stripe hydrogel was also assembled using a sandwich arrangement (Figure 3.4b). A hydrogel band with a thickness of 1 mm was inserted in between two strip electrodes. Square models, 1 mm thick, were utilised to analyse cyclic compression in a traction machine (Figure 3.4c), while dog bone-shaped samples with an electrode at each end wre constructed for cyclic tensile experiments (Figure 3.4d).

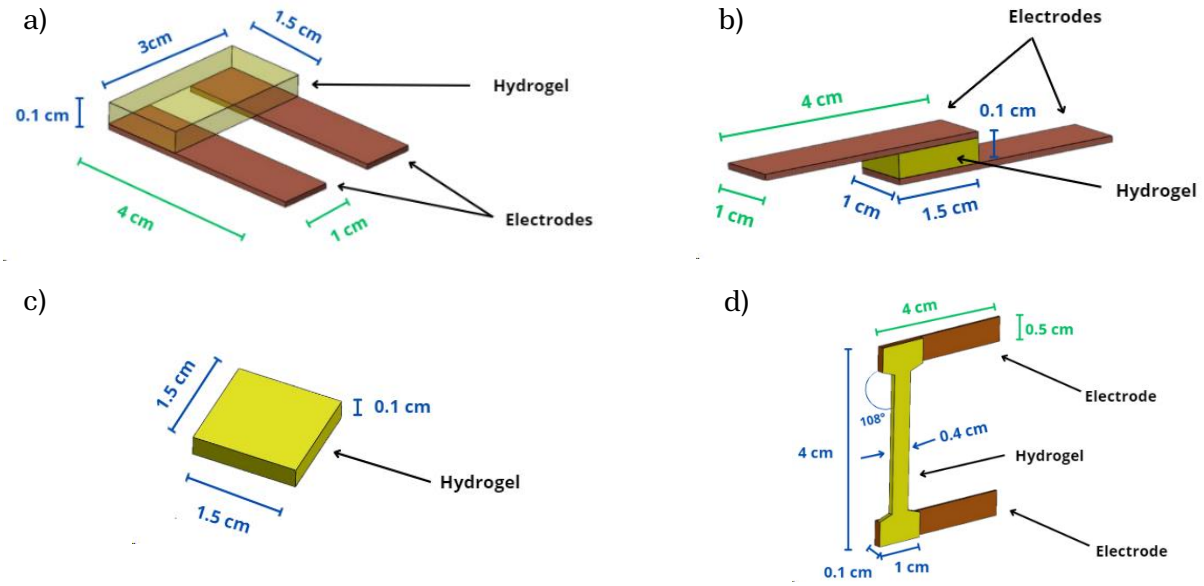

Figure 3.4. *Designed sensor configurations: (a) Parallel model, (b) Sandwich-like model, (c) Square model and (d) Dog-bone model.*

Once the models were established, the formulation was poured into the PDMS moulds, which were then placed inside a chamber and exposed to radiation using an ultraviolet (UV) light lamp (69910 Mercury Arc Lamp Power Supply). Each sample was irradiated for 4 minutes at 200W. The exposure was made in the presence of nitrogen to avoid the radical scavenging that can cause oxygen. The electrodes were attached to the hydrogel on the part not subjected to radiation using a drop of formulation as a glue, and then were exposed for another 4 minutes. The radiation system is shown in Figure 3.5.

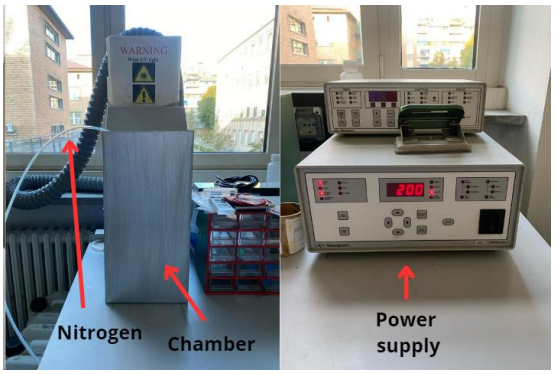

Figure 3.5. *Radiation system for UV light exposition.*

PDMS moulds to shape sensors were made by casting, using PMMA negative moulds prepared with milling machine. Figure 3.6 presents the PDMS moulds used to cure the hydrogel, as well as the samples obtained after UV light polymerization with their respective

electrodes. For the sensor with sandwich configuration, a band was reticulated with the mould of Figure 3.6a and the hydrogel was cut with a cutter to form a strip of 1cm wide, 1.5 cm long and a thickness of 0.1 cm as illustrate Figure 3.6d. The samples were stored inside a petri box with paper soaked in distilled water and then reserved inside a refrigerator so they could maintain their properties and prevent them from drying out. Samples were made with each of the salts and for each of the configurations mentioned above.

3.3. Diffusivity of the salts within the hydrogel

Electrochemical impedance spectroscopy (EIS) is a test in which a system is subjected to an alternating current as a function of frequency to study the electrochemical properties of materials. This type of test was used to study the interaction of the salts contained within the hydrogel with the Kapton-copper electrodes. An impedance measurement was carried out and then the results were subjected to a fitting based on an experimental circuit model. For the test, sensors with a parallel configuration were used, this time with very small electrodes separated by a distance of 10 um, with the aim of avoiding noisy responses. After fitting, the diffusivity and contact resistance parameters of each of the conductive salts were extracted.

3.4. Sensor characterization

In order to characterise the sensor, samples containing the previously mentioned salts underwent traction, compression, and vibration testing, which allowed to examine how the various moving ions behaved. A Keithley multimeter was used to track the voltage and current electrical responses during each test. Data acquisition and parameter settings were executed using LabView. To further examine the diffusivity of ions, the response in time was inspected while a constant force was applied. Finally, a variety of biometric measurements were taken on the body using the best-performing hydrogel as a self-powered sensor.

3.4.1. Compression test

First, it was verified whether the sensor responded electrically to a mechanical stimulus. Consequently, a sample with LiCl in parallel configuration was subjected to cyclic compression. The dimensions of the band remained the same, however, the strips of the copper electrodes became thinner (width 0.5 cm) to evaluate the electrical response of the sensor under a deformation at 5 different points along the hydrogel (Figure 3.7a). Compression tests were performed with the Tensile Test Z5 machine and was controlled trough the THSSD program.

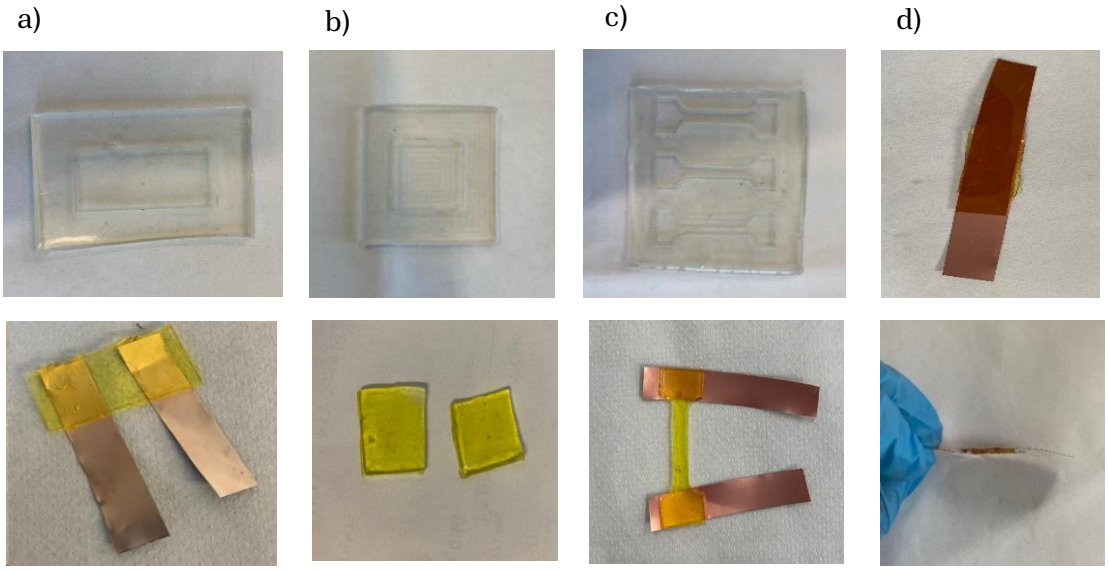

Figure 3.6. *(a-c) PDMS moulds for each configuration (top) and sensors after curing and assembly (bottom). (d) Sandwich-like sensor assembly.*

The sensor was glued to a support on the lower grasp of the machine using a bi-adhesive and the electrodes were clamped to the Keithley 2400 multimeter to measure voltage and current during each test and in each zone of the sensor. A 3D-printed indenter tip with an area of 1cm X 0.5cm (Figure 3.7b) was used to locally apply the compression and it was fitted on the top clamp. On each zone 10 compression cycles were applied at a speed of 10 mm/min and with a force of 50N per cycle.

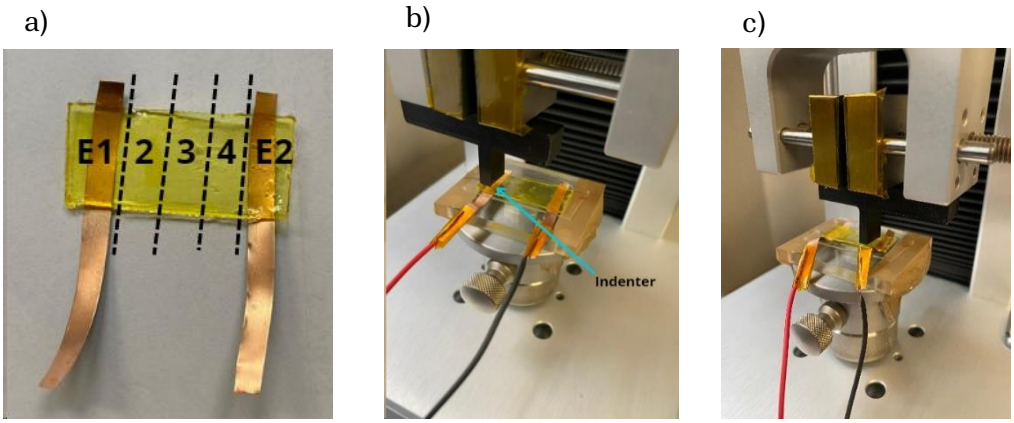

Figure 3.7. *(a) LiCl sample in parallel configuration with contact areas shown. (b-c) Assembly with the sensor on the lower grasp with the indenter and its movement along the hydrogel band.*

Additionally, compression tests were conducted by varying the test's speed and force, in order to analyse ionic movement at high and low speeds, as well as at different loads. Using the model shown in Figure 3.4a, these were applied to samples of various salts in a parallel setup. In this instance, 10 cycles were likewise carried out for every test, and since the

indenter tip was not moved, just one electrode received the deformations for each test. Table 3.3. Force and speed values used in compression tests on parallel and sandwich sensors. lists the force and speed numbers that were employed in the compression experiments. For each of the force both speed values were tested, this was done for each salt.

Force (N)	Speed (mm/min)
50	2.5
100	10

Table 3.3. *Force and speed values used in compression tests on parallel and sandwich sensors.*

In the case of compression with sandwich-like sensors, the square-shaped samples were used. Two strips of conductive tape were used as electrodes that were adhered to the upper and lower grasp of the machine and the sample was arranged between both to exert pressure on it, as shown in Figure 3.8. Assembly for cyclic compression on samples in sandwich configuration.The parameters used were the same used with the sensor in parallel.

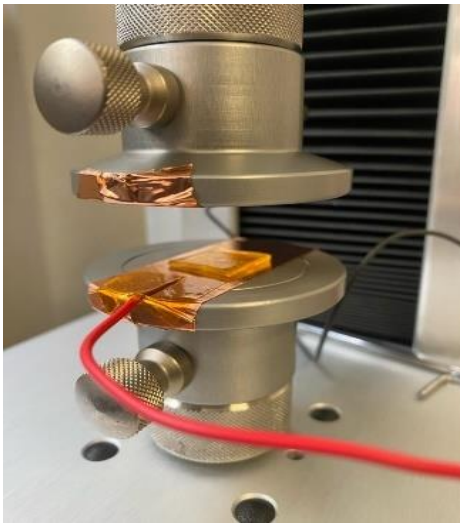

Figure 3.8. *Assembly for cyclic compression on samples in sandwich configuration.*

Furthermore, an analysis of the time constant was accomplished by imposing a continuous force of 80N for 4 minutes on the square-shaped samples, using the previous assembly. The current was measured by each of the salts and then by OriginLab an exponential fitting was performed to obtain the final value of the time constant. The function used was the One-phase exponential decay function with time constant parameter, defined by the following formula:

$$y = y_0 + A_1 e^{-x/t_1} \tag{3.1}$$

3.4.2. Vibration test

A dynamic investigation at various frequencies and forces was conducted using the TIRA vib, also referred to as "Shaker". This device simulates a vibrating environment under various conditions by an electromechanical actuator. A metal bar that was movable by a knob was fitted in order to conduct the electromechanical tests (Figure 3.8a). To determine the strength and acceleration with which the bar would strike the sample, a force sensor and an accelerometer were mounted to the shaker (Figure 3.8b). The vibrating system was controlled by the VibrationVIEW program, in which it was possible to set the displacement of the shaker and the vibrating frequency, as well as to monitor the force and acceleration exerted on the sample. To record both current and voltage, the Keithley 6517B electrometer was used to track the dynamic behaviours of both signals.

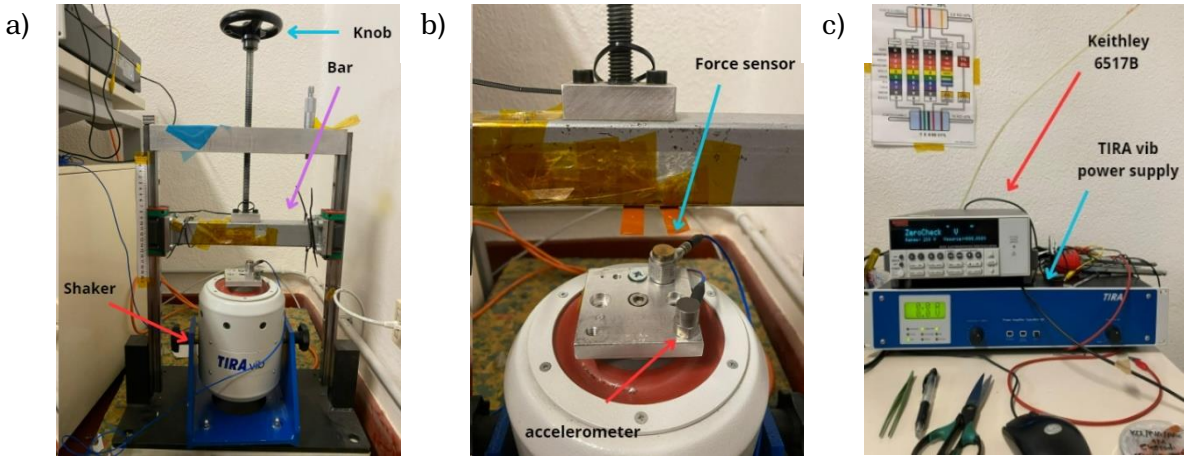

Figure 3.9. *(a) Vibration test system. (b) Accelerometer and force sensor on the shaker. (c) Keithley electrometer and TIRA vib control system.*

Both sandwich and parallel sensor types were subjected to these tests. Small sensors in Figure 3.6d were used for the sandwich configuration. Small model sensors in Figure 3.6d were used for the sandwich configuration. The hydrogel was bonded with bi-adhesive on the top of force sensor as shown in Figure 3.9a. Since the parallel sensor was too big to fit over the force sensor, it was attached to the bottom of the metal bar using bi-adhesive so that the force sensor could come into contact with one of the hydrogel electrodes (Figure 3.9b).

a) 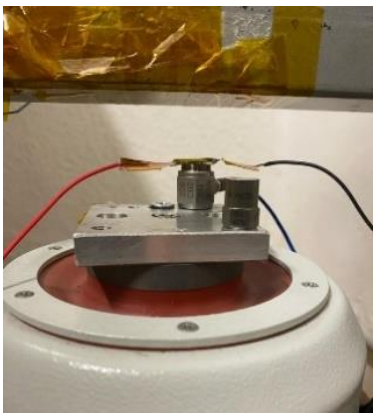 b) 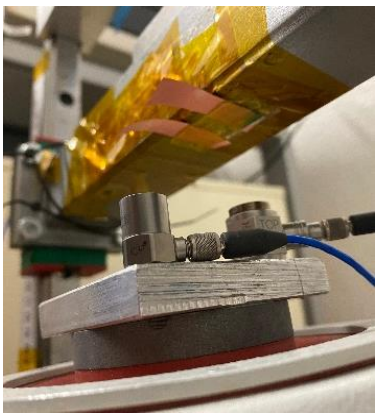

Figure 3.10. *(a) Sandwich sensor assembly for the frequency test. (b) Parallel sensor assembly for the frequency test.*

The frequency and force parameters used during the tests are presented in Table 3.4. Force and frequency values used in vibration tests on parallel and sandwich sensors.. It started with a constant force value of 10 N and was tested at different frequencies, then the force was increased to 30 N and the frequencies were changed again, the previous was done for each of the salts.

Force (N)	Frequency (Hz)
10	1
30	2.5
-	4

Table 3.4. *Force and frequency values used in vibration tests on parallel and sandwich sensors.*

3.4.3. Tensile test

The piezoionic effect was also studied under traction movements using an Instron tensile machine with a load cell of 10 kN. The dog bone-shaped samples edges were grasped to the lower and upper clamps of the device. The lower clamp remained fixed while the upper clamp was displaced at different speeds and at different deformation ranges (Figure 3.10. (a) Sandwich sensor assembly for the frequency test. (b) Parallel sensor assembly for the frequency test.). As in previous tests, current and voltage were recorded, this time using the Keithley 2400.

Figure 3.11. *Assembly for tensile tests using dog bone shaped samples.*

High speeds were used for these tests because at low speeds and smooth movements, the sensor response tends to be very small and difficult to monitor. Table 3.5 shows the established velocity and deformation values. New samples were used for each of the tests and for each of the salts. Strain and strain data were then related to electrical responses obtained with the sensor.

Speed (mm/min)	Strain (%)
200	20
500	50
-	80

Table 3.5. *Speed and deformation values used in tensile tests on dog-bone shaped sensors.*

Chapter 4.

Results

4.1. Recognition of the output waveform

In order to check whether the sensor reacted electrically to the deformations, a cyclic compression was applied to a sample with parallel configuration as shown in Figure 3.7. (a) LiCl sample in parallel configuration with contact areas shown. (b-c) Assembly with the sensor on the lower grasp with the indenter and its movement along the hydrogel band.a. The sample contained LiCl, and the stimulus were applied in 5 different areas of the sensor. The results obtained for the current are shown in Figure 4.1. In general, the output waveform of the current and the voltage has a periodic shape with positive and negative peaks.

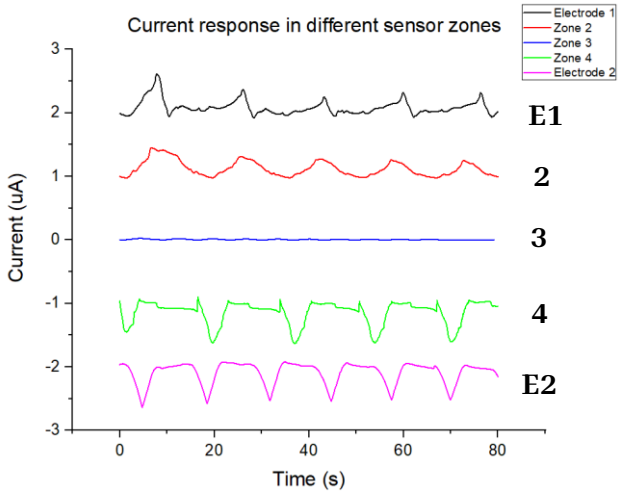

Figure 4.1. *Current response to a cyclic compression in different sensor zones.*

According to the results in Figure 4.1, once the stimulus is applied, the current begins to grow until the load is released, then the hydrogel begins to recover from the deformation and the current decreases. It is also evident how the electrical response is influenced by the distance between the electrodes and the load. The current is stronger and has a more defined form when the deformation is applied to the electrodes or very near to them. Because of the charge of the ions, it is also possible to determine the direction in which the force has been applied. As shown in Figure 4.1, a positive deformation is placed on electrode 1 and tends to become negative as the source gets closer to electrode 2.

4.2. Diffusivity

By fitting with the electrical model, it was also possible to know the diffusivity constant of each of the salts, as well as the contact resistance with respect to the Kapton-copper electrodes. Table 4.1 presents the experimental values of the radius of each of the ions used,

while Table 4.2 presents the values obtained for the diffusivity and contact resistance parameters from the EIS analysis.

Ion	Radius (nm)
Lithium (Li)	0.069
Sodium (Na)	0.102
Potassium (K)	0.138
Rubidium (Rb)	0.149
Chlorine (Cl)	0.181

Table 4.1. *Radii of the ions that compound the salts [85]*

Compound	Diffusivity (cm^2/s)	Contact resistance (Ω)
LiCl	5.64E-07	5.6E+09
NaCl	4.85E-07	3.723E+08
KCl	4.86E-08	4.19E+07
RbCl	6.27E-08	7.52E+07

Table 4.2. *Diffusivity and contact resistance values for each of the salts used.*

With regard to diffusivity, it is evident that the salts with the smaller and less heavy ions possess the ability to move faster through the hydrogel while the larger ones present a higher difficulty, however, according to the contact resistance results, when the electrodes are very close to each other and the space is reduced, the heavier salts like the RbCl and KCl possess a lower resistance to the flow of the current as opposed to smaller salts. In that sense, it is possible that the salts composed of lithium and sodium tend to stay close to the copper electrodes when external stimuli are applied.

4.3. Compression tests

Compression tests were performed by 10 cycles at forces of 50 N and 100 N and speeds of 2.5 mm/s and 10 mm/s on samples containing the different salts and reference samples without salt. The current and voltage waves resulting from tests with parallel and sandwich configurations are shown in Figure 4.2.

At first glance, the waves are more defined in the sandwich configuration, likewise, in this configuration, the electrical responses are more intense than the parallel configuration. The sample with the LiCl seems to have the best performance for the current as the voltage in the case of the sensors with the electrodes in parallel configuration, contrary to the case of the sandwich electrodes, where the RbCl has the most dominant response. In order to quantify the current and voltage values, a statistical analysis was performed as shown in Figure 4.3, where the bars represent the mean with their respective standard deviation. Figure 4.3 presents the current responses in each of the configurations using all the salts and reference, plus a comparison at different speeds and forces. It is important to mention that the electrical response of the reference is different from zero because the carboxylic groups present in the acrylic acid dissociate during polymerization, some of these groups bind to

the PVA polymer chain while some hydrogen ions remain free and mobile within the hydrogel.

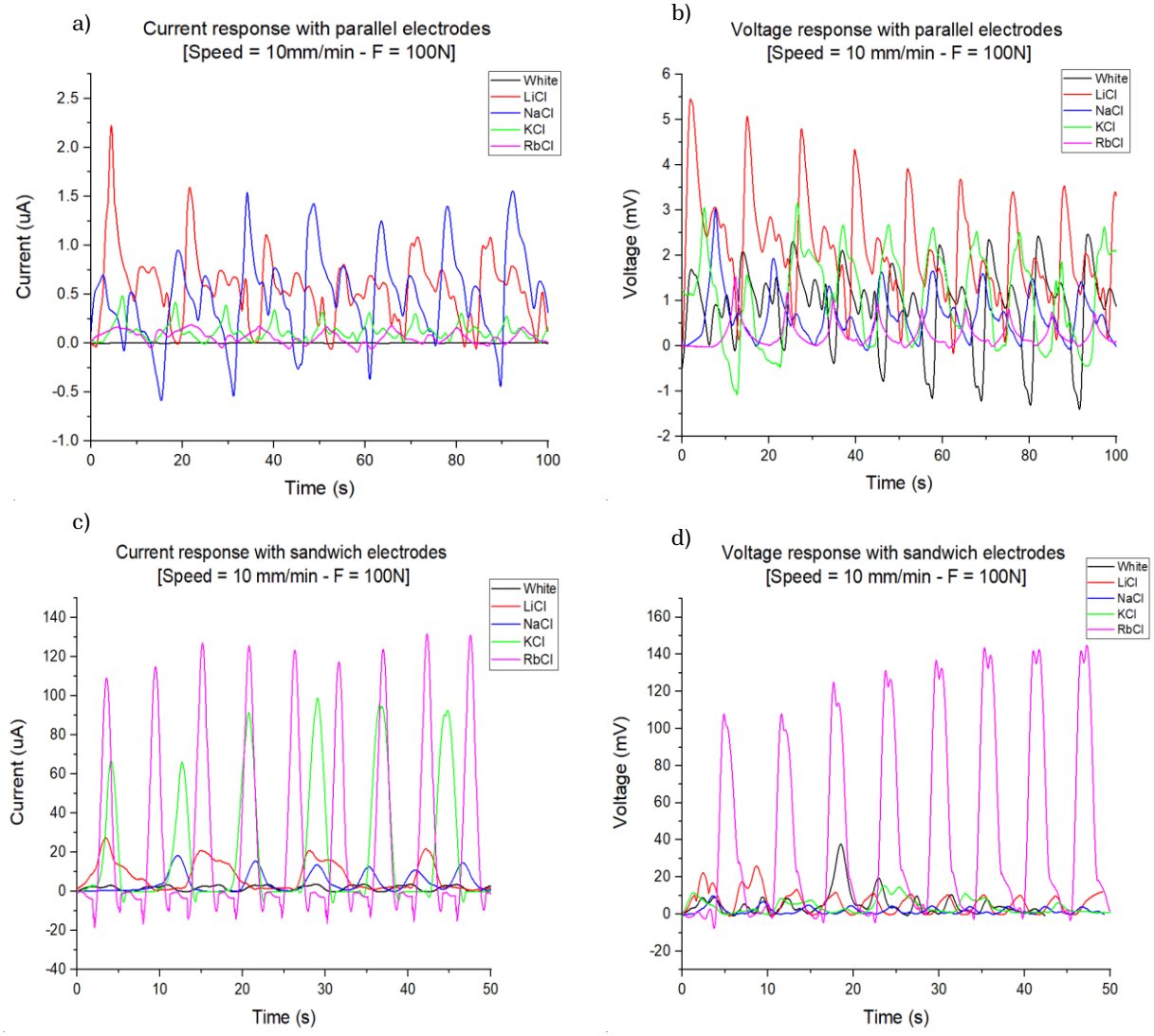

Figure 4.2. *(a) Current and (b) voltage output waves on sensors with parallel electrodes and (c) current and (d) voltage with sandwich electrodes at a force of 100N and a speed of 10 mm/min.*

Comparing both configurations, the effect of distance is much more evident. When there is a bigger gap between the electrodes, the response is less intense than when they are closer. Salts with smaller ions such as LiCl and NaCl have better performance in parallel configuration, which may be due to their diffusivity (Table 4.2), these have the ability to move with less difficulty and faster through the polymer, however, in the sandwich configuration it seems that the contact resistance has a more dominant effect on the response, since the sensors containing the heavier salts have a better performance. With respect to the change in speed, as it increases, a higher response is obtained in the parallel configuration, while with the sandwich electrodes the response is reduced almost in half for all samples. With the change of force, it can be deduced that as a force greater is used, the response tends to grow in both configurations.

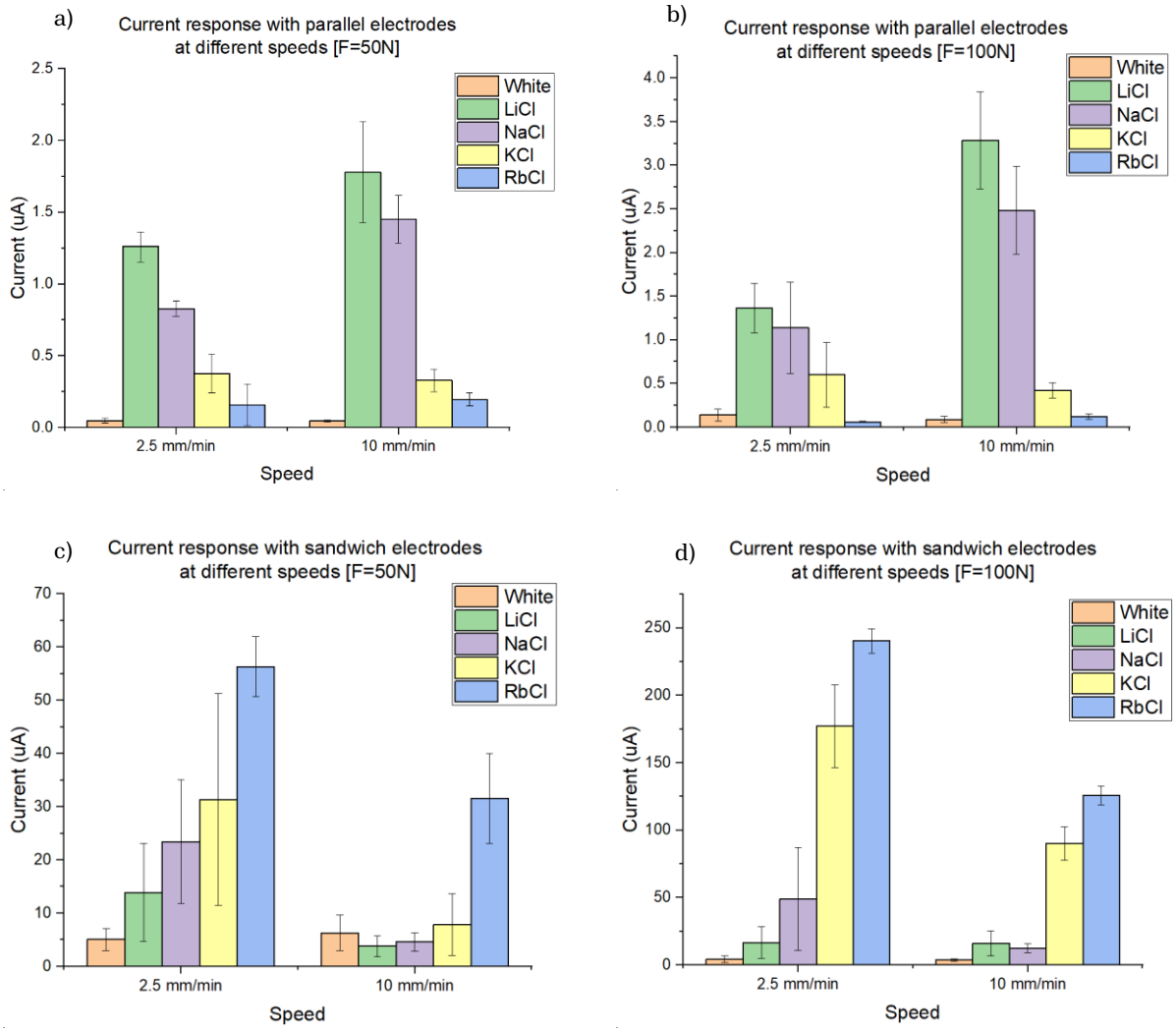

Figure 4.3. *Current statistics with parallel configuration (top) and sandwich configuration (bottom) at different speeds. (a, c) with a force of 50 N and (b, d) with a force of 100 N.*

As shown in Figure 4.4, the voltage in sensors in parallel configuration tends to have the same behaviour as the current in terms of salts and force, that is, increases with force and samples with smaller salts perform better, yet, as the speed increases it begins to decrease. In the case of sandwich configuration, although the sensor with RbCl has the best performance, the voltage fluctuates among the rest of the salts at different speeds but tends to grow with the application of higher forces.

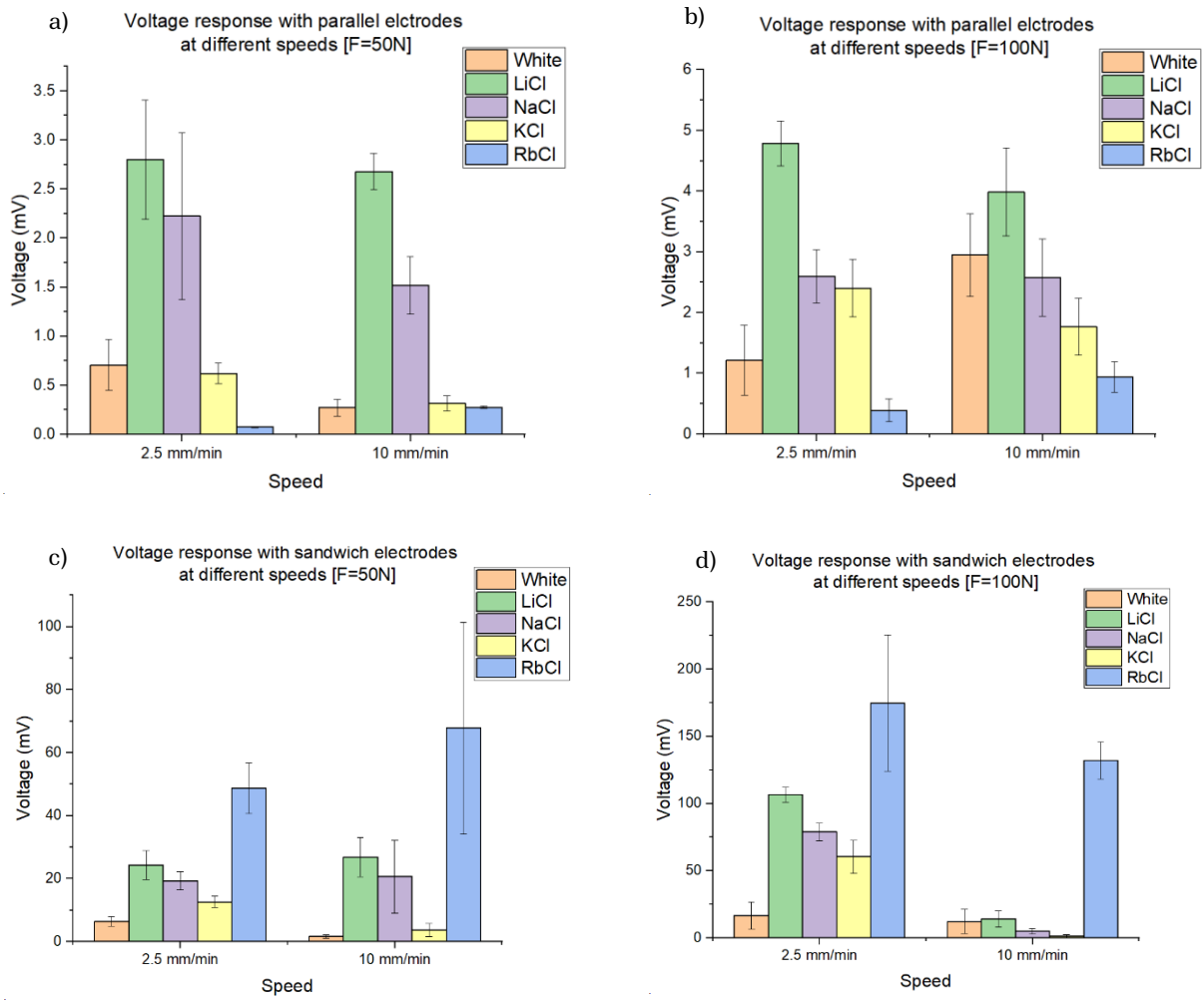

Figure 4.4. *Voltage statistics with parallel configuration (top) and sandwich configuration (bottom) at different speeds. (a, c) with a force of 50 N and (b, d) with a force of 100 N.*

From the mechanical data obtained with the compression test, a decay of the electrical response can be seen for each cycle, both in current and voltage, due to the viscoelastic behaviour of the hydrogel, which fails to recover its initial form completely after each deformation. In Figure 4.5a the stress-strain curve of one of a sample with RbCl is illustrated, in which the first cycle is in which the greatest deformation is reached and then begins to decrease, in Figure 4.5b and Figure 4.5c the current decay of the sensor at different forces is more clearly presented.

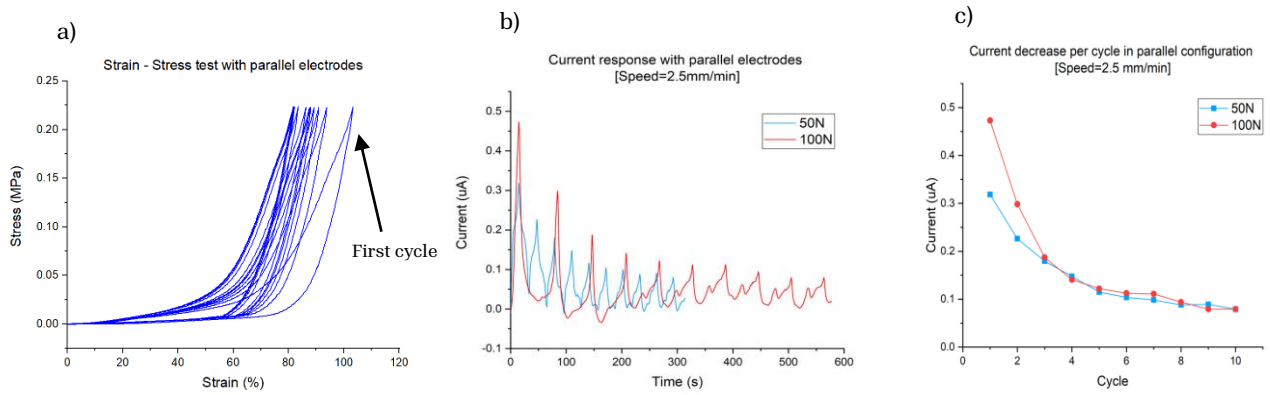

Figure 4.5. *(a) Stress – Strain curve for 10 compression cycles on a sensor with parallel configuration. (b) Current response with parallel electrodes at different forces. (c) Current decrease per cycle in sensor with parallel configuration.*

4.3. Vibration tests

The samples in sandwich and in parallel configurations were tested with the shaker at frequencies of 1 Hz, 2.5 Hz and 4 Hz and forces of 10N and 30N. The input signals of the acceleration and force controlled with the VibrationVIEW program are shown in Figure 4.6, while Figure 4.7 presents both current and voltage output signals of both configurations at frequency of 2.5Hz and 10N force.

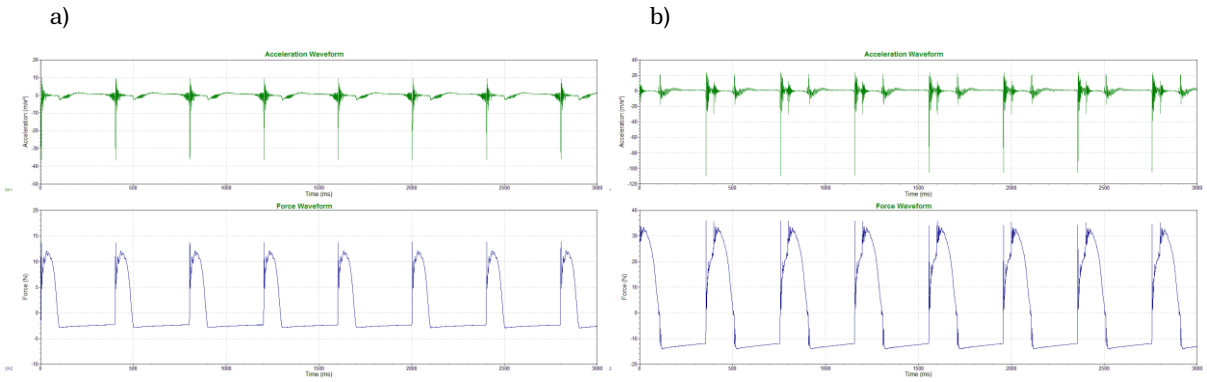

Figure 4.6. *(a) Acceleration waveform (top) and force waveform at 10N (bottom) and (b) acceleration waveform (top) and force waveform 30N (bottom).*

The output waveforms of voltage and current are illustrated in Figure 4.7, where it can be appreciated the high speed and constancy with which the deformations are applied contrary to the cyclic compression test which is slower. The waveform also tends to be periodic but in this case the wave tends to remain and there is no decay of the electrical signal in time.

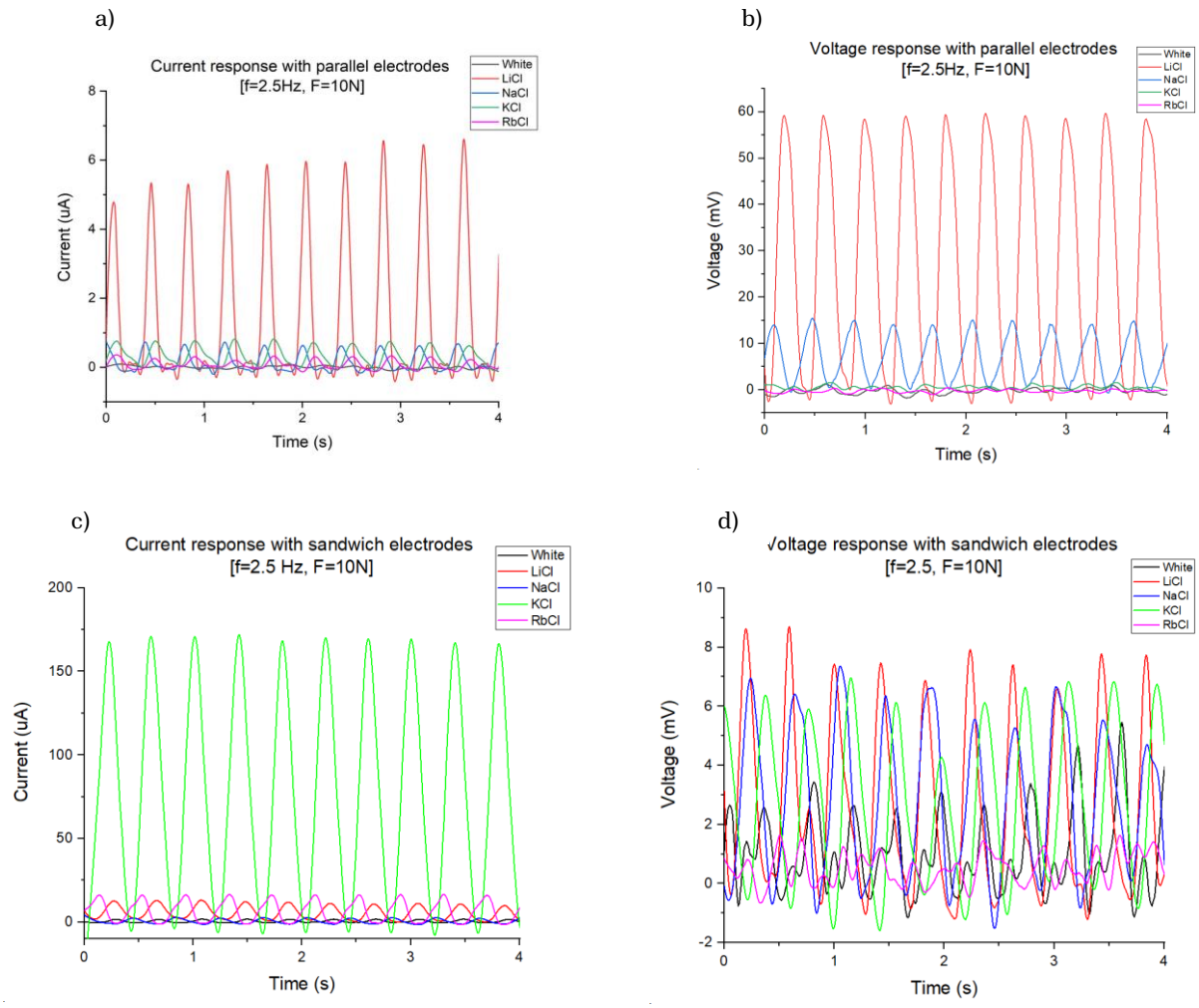

Figure 4.7. *(a) Current and (b) voltage output waves on sensors with parallel electrodes and (c) current and (d) voltage with sandwich electrodes at a force of 10N and a frequency of 2.5 Hz.*

On the other hand, from the statistical data presented in Figure 4.8 and Figure 4.9 for current and voltage respectively, it can be deduced that sensors with parallel configuration have a very similar behaviour to those subjected to compression. In this case the diffusivity of the smaller ions predominates and are the samples with the best performance, while the response decreases when salts with larger compounds such as KCl and RbCl are used. For both configurations, the current grows with strength and with frequency. In the sandwich configuration, the effect of the contact resistance mentioned above can be seen more clearly. The highest response in samples with nearby electrodes is gotten with KCl, salt with the lowest contact resistance and the smallest response is obtained with LiCl, which is the salt with the highest resistance. Sensors with LiCl and KCl have the best current performance in parallel and sandwich configuration respectively.

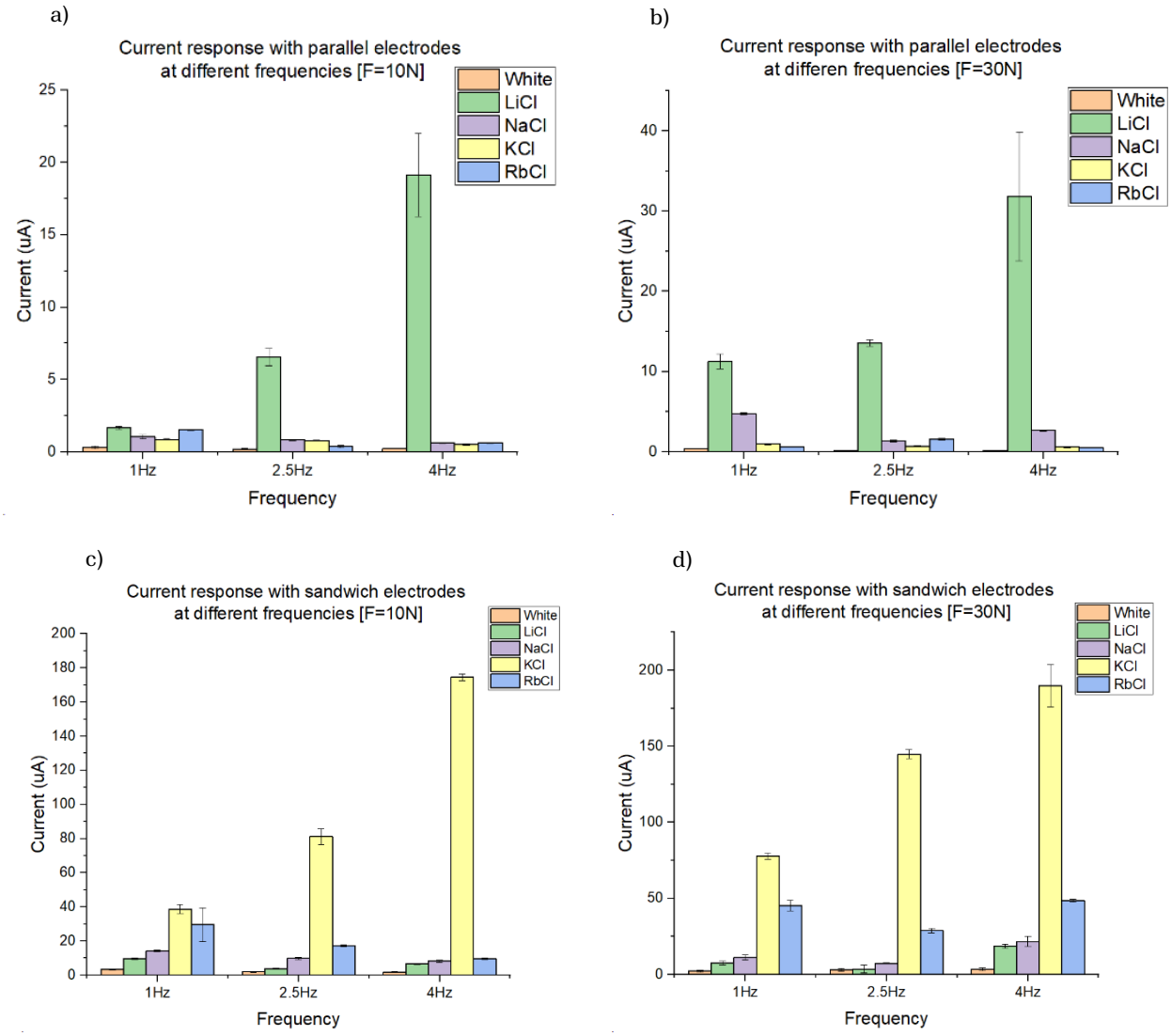

Figure 4.8. *Current statistics with parallel configuration (top) and sandwich configuration (bottom) at different forces. (a, c) with a force of 10 N and (b, d) with a force of 30 N.*

The voltage for parallel sensors appears to saturate and decrease for frequencies above 2.5 Hz. In sandwich sensors there is no greater difference between the frequencies of 1 Hz and 2.5 Hz, while with a high frequency of 4 Hz the voltage increases by a large amount. In general, higher forces make a higher response possible. The voltage in the sample with the LiCl is much more intense than the other salts and the sensors with RbCl have the lowest performance.

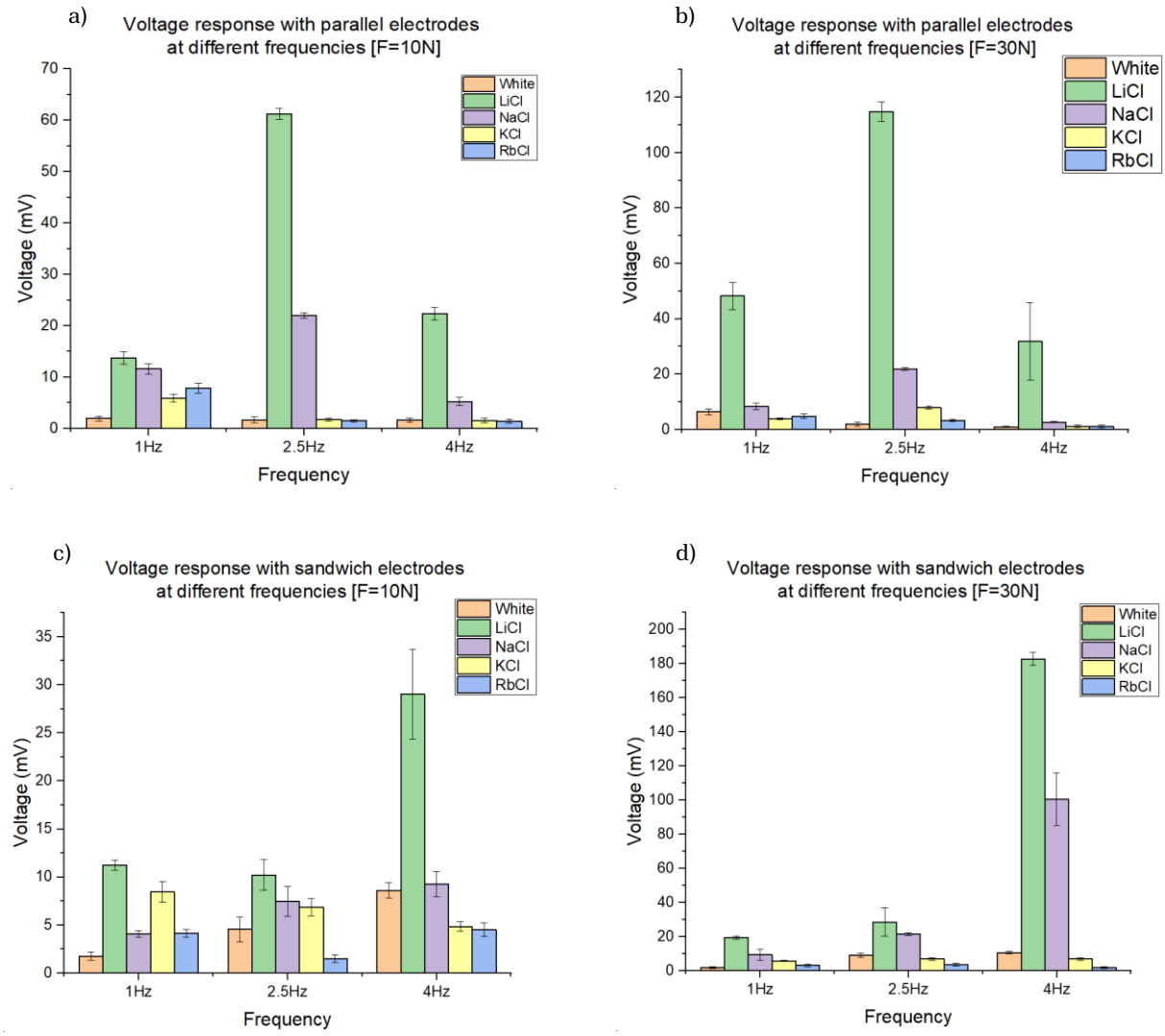

Figure 4.9. *Voltage statistics with parallel configuration (top) and sandwich configuration (bottom) at different forces. (a, c) with a force of 10 N and (b, d) with a force of 30 N.*

4.3. Tensile tests

The dog bone-shaped sensors were subjected to tensile testing using speeds of 200 mm/min and 500 mm/min, as well as deformations of 20%, 50% and 80%. In the current and voltage output waveforms shown in Figure 4.10 it can be seen that at low speeds (200 mm/min) the cyclic wave has a triangular shape, where the lower peaks represent the moment when the hydrogel stretch begins while those that are higher represent the recovery of the sensor shape. Unlike compression, waves do not decrease with cycles, however, when the speed increases to 500 mm/min the triangular wave shape is lost and tends to become a sine wave.

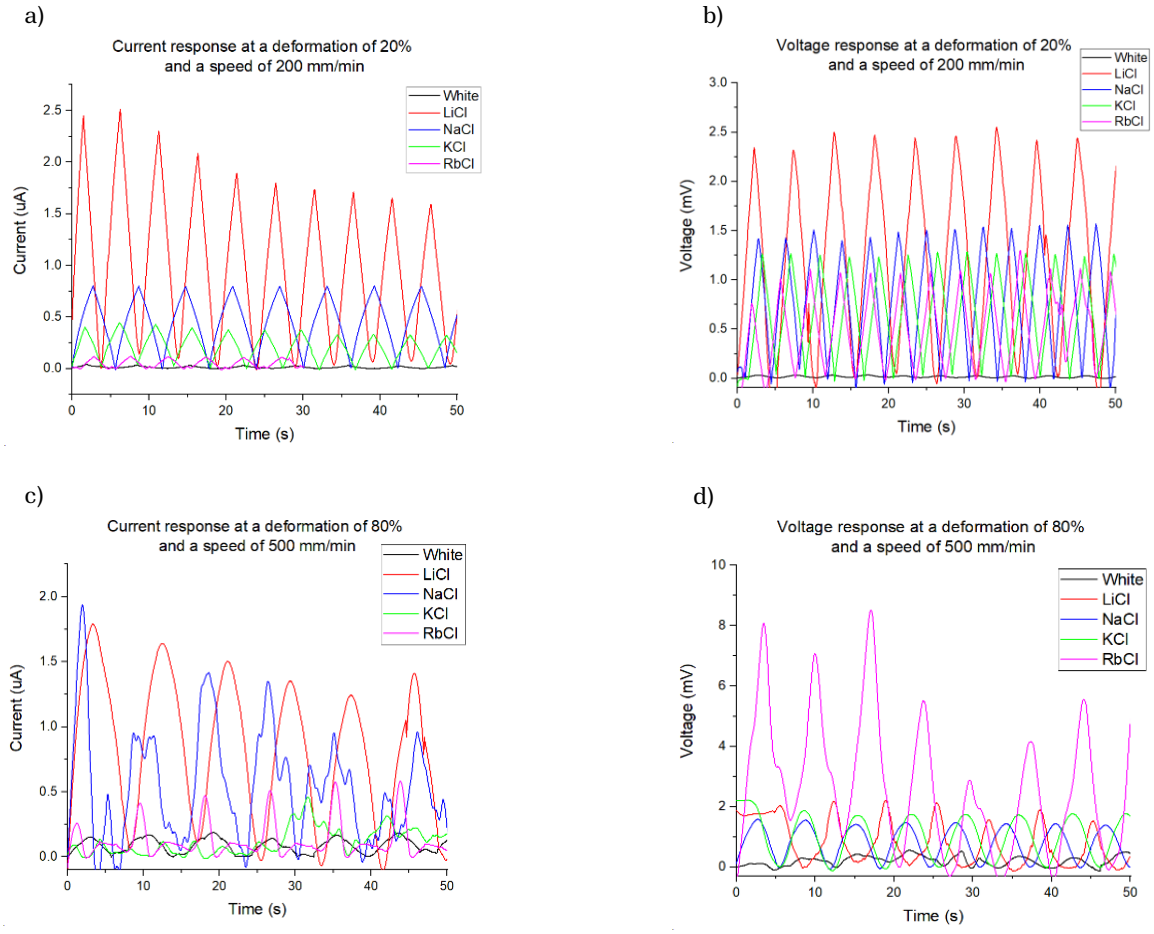

Figure 4.10. *(a) Current and (b) voltage output waves on sensors subjected to a tensile test at a deformation of 20% and a speed of 200 mm/min. (c) Current and (d) voltage output waves on sensors subjected to a tensile test at a deformation of 80% and a speed of 500 mm/min.*

The average current and voltage levels achieved in the compression and vibration tests are significantly higher than those shown in Figure 4.11 statistical data for the tensile test. Since the signals in traction are very low, very high speeds deformation rates are required to achieve a reaction on the scale of micro amperes and millivolts. When it comes to current, the sample containing LiCl yields the best results, followed by sensors containing NaCl, KCl, and RbCl, in that order. Applying strains than more than 50% results in a significant drop in current. Similarly, the current decreases with increasing speed. The voltage exhibits distinct behaviour; at 200 mm/min, the optimum reaction is reached at 50% deformation, and there is little discernible difference between the 20% and 80% deformations. RbCl samples show the highest values of the contact resistance effect, which appears to take over from the diffusive effect as velocity increases.

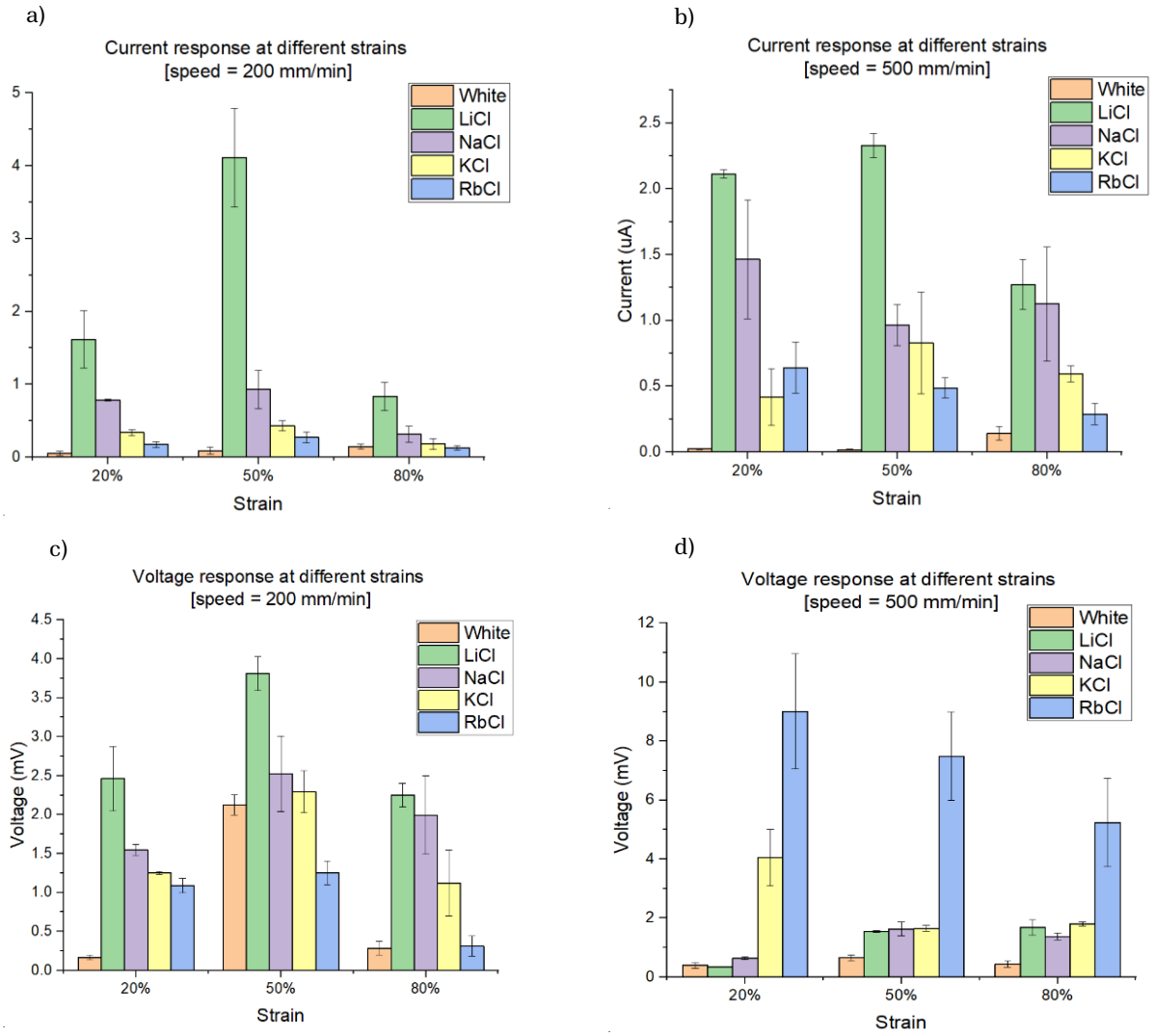

Figure 4.11. *Current (top) and voltage (bottom) statistics from the tensile test at different strains, (a, c) with a speed of 200 mm/min and (b, d) with a speed of 500 mm/min.*

4.4. Time constant

In order to know how long the current takes to return to a state of equilibrium after a deformation, each of the sensors with the square-shaped configuration were subjected to a compression with a constant force of 80N for 4 minutes. The test performed on samples with each of the salts. Figure 4.12 shows the results obtained for each of the salts and the fitting carried out with the OriginLab program and Table 4.3 shows the values obtained after fitting. According to the values obtained, the constant time tends to increase with size of the ions, and it is evident that this parameter has a great influence on the electrical response, in this case, the LiCl salt has the smallest time constant, so the response tends to be faster with sensors containing this type of compound. The behaviour is followed by the NaCl, then the KCl and finally the RbCl, which is the heaviest salt and the one that takes more time to return to balance.

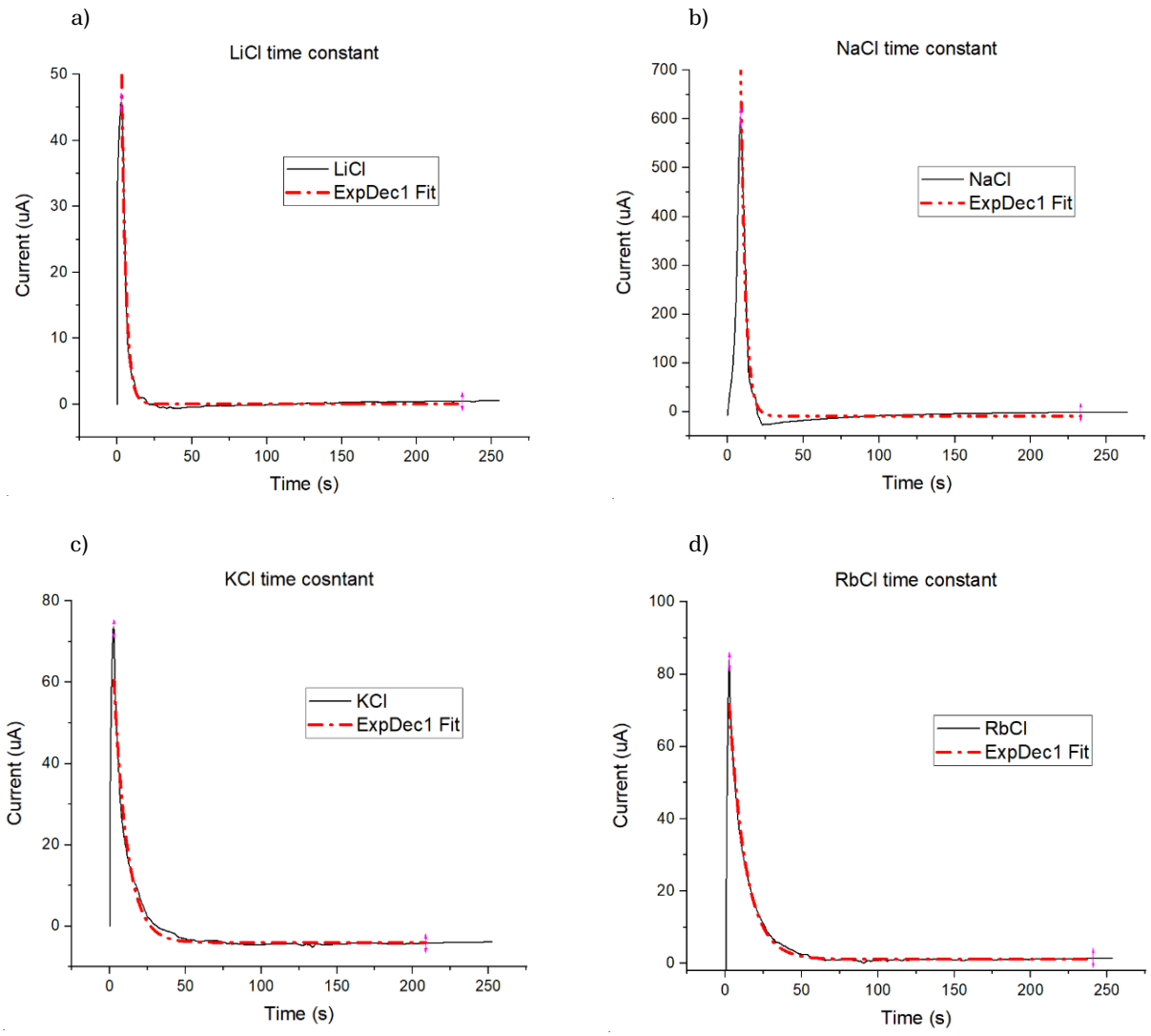

Figure 4.12. *Current time constant response (a) LiCl, (b) NaCl, (c) KCl and (d) RbCl.*

Salt	Time constant (s)
LiCl	2.87
NaCl	3.11
KCl	8.74
RbCl	10.02

Table 4.3. *Time constant values for each of the salts.*

4.5. Applications

Finally, samples that gave the most stable and high-value response in current and voltage were used to perform various biometric measurements in the human body and confirm the effectiveness of the sensor. As a result, sensors with a parallel arrangement and LiCl as a conductive salt were chosen. To measure current and voltage during the opening and closing of the hand, the electrodes were first attached to the Keithley 2400, and the sensor was initially placed on a subject's wrist (Figure 4.13a), then the wrist and the sensor were covered

with parafilm to reduce rumour and improve the adhesion of the device to the skin. The voltage and current responses are shown in Figure 4.13b and Figure 4.13c, respectively. In them it can be appreciated the sinusoidal waves characteristic of the piezoionic response, and it is possible to identify the moment in which the hand closes with the lowest peaks and when the hand opens on the highest peaks.

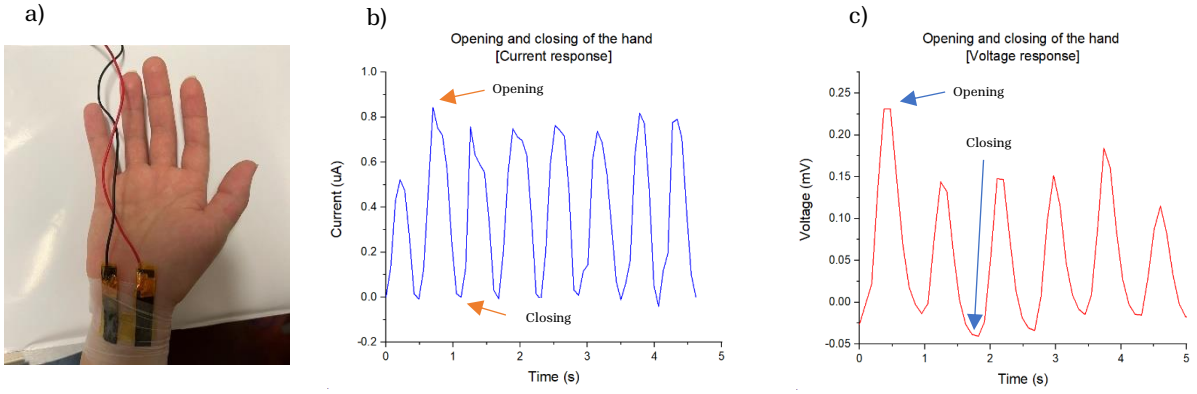

Figure 4.13. *(a) Positioning the LiCl sensor on the wrist. (b) Current wave in time during hand opening and closing. (c) Voltage wave in time during hand opening and closing.*

The sensor was also placed around the index finger to monitor the finger bending at different intensities. Figure 4.14b shows the voltage signal obtained where the number of folds made with the finger and the constancy and repeatability with which the movement is made can be identified.

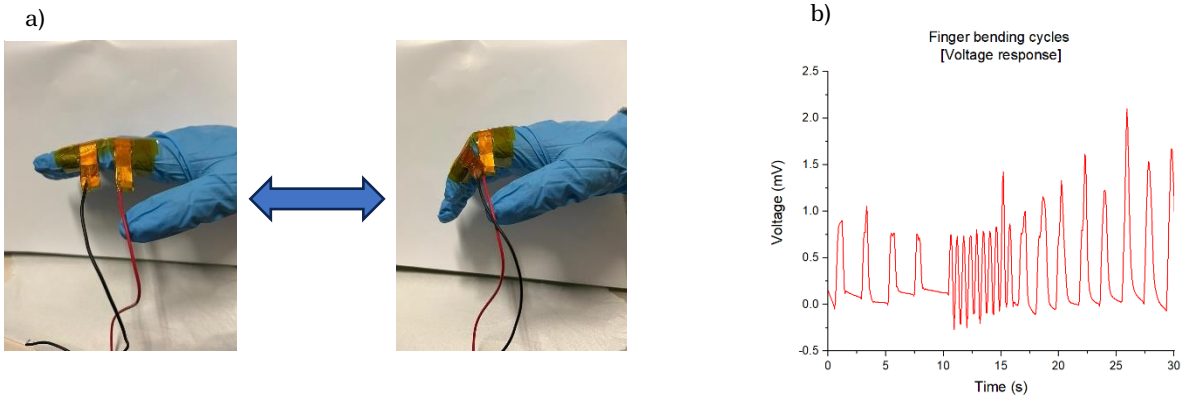

Figure 4.14. *(a) Positioning the LiCl sensor on the index finger to monitor the bending. (b) Voltage wave in time during hand the finger bending.*

Finally, voice monitoring was performed. The sensor was placed over the throat to monitor the vibration of the voice while a person uttered words. Figure 4.15 identifies the moments in which the pronunciation and the constancy of the uttering is performed.

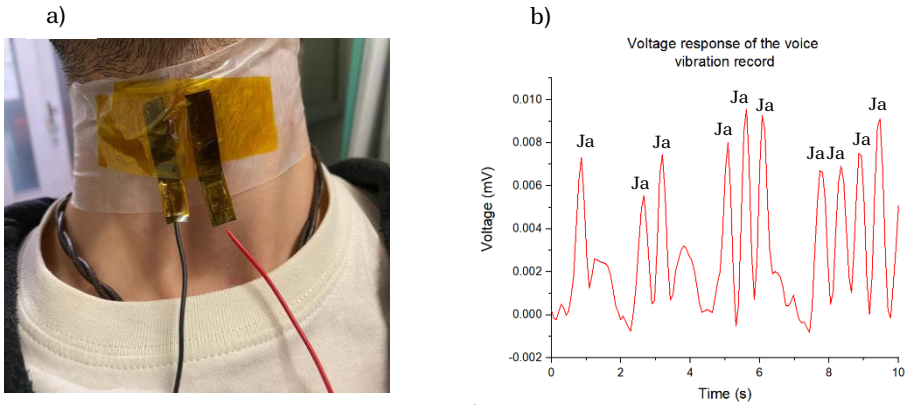

Figure 4.15. *(a) Positioning the LiCl sensor on the throat to monitor the vibration of the voice while speaking. (b) Voltage wave in time during hand the pronunciation of words "Ja", "Ja Ja", "Ja Ja Ja" and "Ja Ja Ja Ja".*

With the results obtained, it was possible to verify that the sensor has the ability to monitor different movements in the human body and perceive different physical stimuli of the environment. In the future it could be used as a tactil biometric sensor useful in the area of health monitoring.

Chapter 5.

Limits and future proposals

The oxidation of Kapton-copper electrodes over time was one of the most common obstacles encountered during the project's development. The humid environment in which the samples were stored to prevent them from drying out caused the electrodes to deteriorate over time (Figure 5.1a). During this study, sensors were attempted using LIG, aluminium and stainless steel electrodes such as those in Figure 5.1b and Figure 5.1c, however, the results were not successful, the electrodes in these materials were very noisy and did not adhere well to the hydrogel, therefore it is necessary to look for a type of electrodes that do not rust in the presence of water, that are resistant and interact well with the polymer. Another alternative may be to work to improve the durability of the sensor so that it does not dry out of the refrigerator.

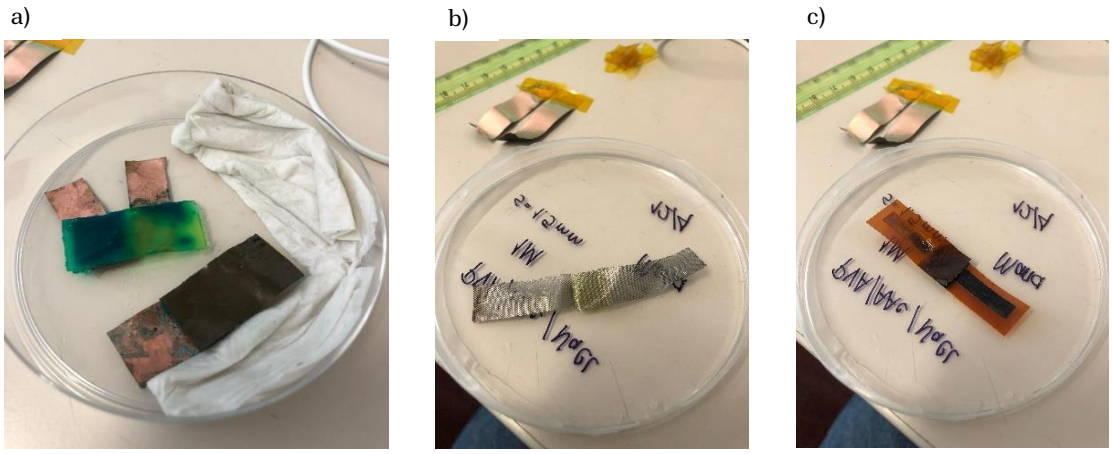

Figure 5.1. *(a) Sensor with Kapton-copper electrodes oxidized by water. Sample with (b) aluminium electrodes and (c) Laser-Induced graphene (LIG) electrodes.*

Distance was one of the most critical parameters in the results obtained. Changing the thickness of the samples and extending the distance between the electrodes may be a future proposal to help better understand the piezoionic effect. During the project some tests were performed on printed 3D structures using the same formulation and using NaCl as conductive salt. The samples were subjected to cyclic compression with a force of 25N and a speed of 50 mm/min. Current and voltage were measured during the tests. The results are presented in Figure 5.2c and Figure 5.2d, respectively. In both cases, the signals were very similar to those obtained with thin sensors and voltage and current values were really high, this give a good indication of the behaviour of thicker sensors that could be used to develop other tactile sensors.

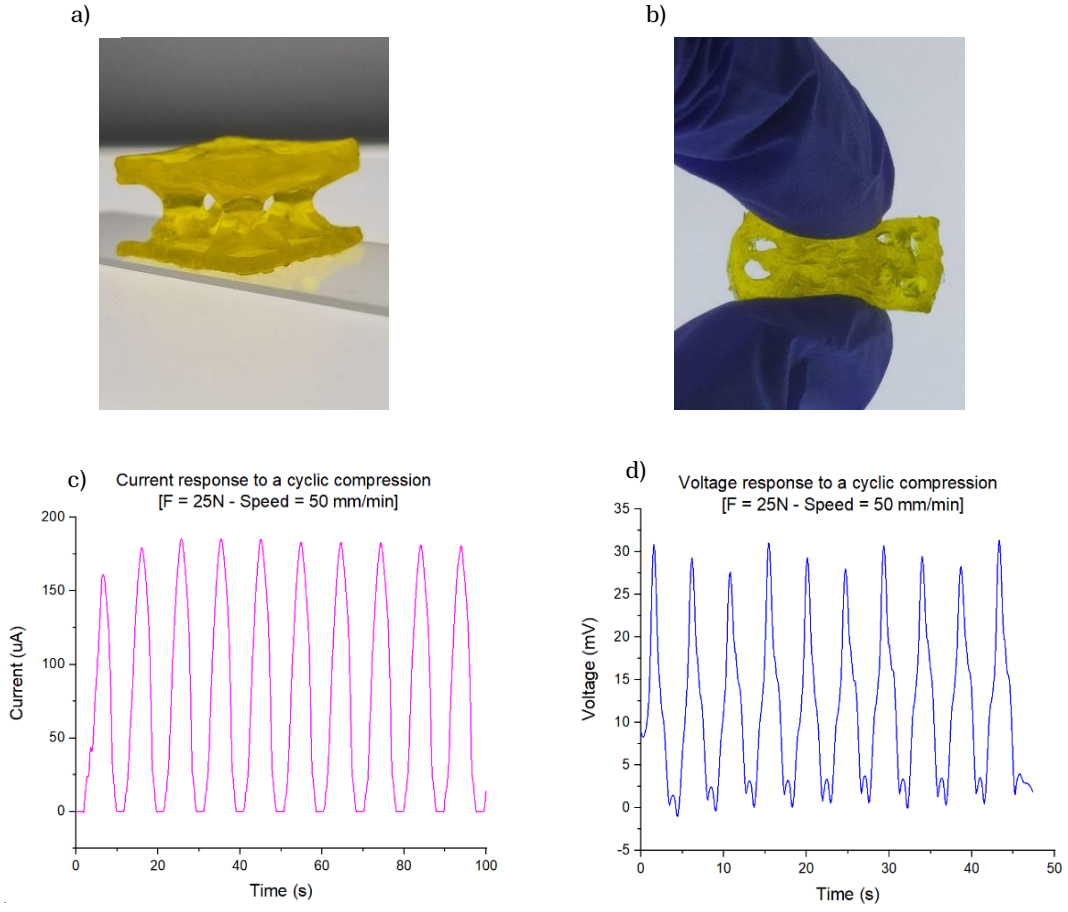

Figure 5.2. *(a-b) Flexible 3D structures printed with NaCl inside. Current (c) and voltage (d) response of a 3D structure subjected to a cyclic compression.*

Conclusion

During this project, an analysis of the piezoionic effect on a photocurable, and self-healing hydrogel was carried out, which after being characterized was used as a biometric sensor for monitoring different human movements. The hydrogel formulation was prepared by mixing distilled water, PVA, PEGDA, AAc, and a photoinitiator. Then, the polymer was crosslinked using an UV lamp in the presence of nitrogenous. The impact of ionic mobility on the electrical response of the material was validated using salts with the same anion but different cation (LiCl, NaCl, KCl, RbCl). For the study of the piezoionic phenomenon, sensors with 4 different configurations were used: parallel, sandwich, square-shaped and dog bone. Kapton-copper electrodes were employed to build the sensors. The diffusivity of the ions and their interaction with the copper electrodes were evaluated by means of Electrochemical Impedance spectroscopy (EIS), with which the diffusivity and contact resistance values of each of the salts were obtained. Salts with smaller ions, like LiCl and NaCl had the highest diffusivity and the largest salts such as RbCl and KCl had the lowest contact resistance. Several mechanical tests were developed to characterize the sensor and during each test, current and voltage were measured using the Keithley mutlimeter in order to study the electrical response of the sensors. In the compression and vibration tests, the diffusivity effect was dominant in the parallel configuration, when there was more distance between the electrodes, the sensors with LiCl and NaCl had a better performance because the ions were smaller. In the sandwich configuration the effect of contact resistance was predominant and the responses with the KCl and RbCl salts were the highest. As for traction movements, the sensor with LiCl inside presented the best current response, while the voltage behaviour depended on the speed. In addition, a study of the time constant of each of the salts was made using a constant force on the samples. The salt with the smallest ion, LiCl, had the lowest value. It was possible to deduce that the value of the time constant increased according to the size of the salt. A sensor with parallel configuration and based on LiCl was used to measure different physiological signals on the human body demonstrating the functionality of the device. Despite some limitations that were presented in the study such as the oxidation of copper electrodes, it was possible to prove and analyse the piezoionic effect and implement it in the development of a self-powered sensor that could be used as a more innovative alternative to the development of new tactile sensors.

Bibliography

[1] D. Deflorio, M. Di Luca, and A. M. Wing, “Skin and Mechanoreceptor Contribution to Tactile Input for Perception: A Review of Simulation Models,” *Frontiers in Human Neuroscience*, vol. 16, Jun. 2022, doi: 10.3389/fnhum.2022.862344.

[2] B. Ying and X. Liu, “Skin-like hydrogel devices for wearable sensing, soft robotics and beyond,” *iScience*, vol. 24, no. 11, p. 103174, Nov. 2021, doi: 10.1016/j.isci.2021.103174.

[3] C. Géhin, J. Tokarska, S. J. Fowler, P. E. Barran, and D. K. Trivedi, “No skin off your back: the sampling and extraction of sebum for metabolomics,” Metabolomics, vol. 19, no. 4, Mar. 2023, doi: 10.1007/s11306-023-01982-3.

[4] K. Johnson, “The roles and functions of cutaneous mechanoreceptors,” *Current Opinion in Neurobiology*, vol. 11, no. 4, pp. 455–461, Aug. 2001, doi: 10.1016/s0959-4388(00)00234-8.

[5] J. Dargahi and S. Najarian, “Human tactile perception as a standard for artificial tactile sensing - a review,” *International Journal of Medical Robotics and Computer Assisted Surgery*, vol. 01, no. 01, p. 23, 2004, doi: 10.1581/mrcas.2004.010109.

[6] X. Wu et al., “A potentiometric mechanotransduction mechanism for novel electronic skins,” *Science Advances*, vol. 6, no. 30, Jul. 2020, doi: 10.1126/sciadv.aba1062.

[7] Y. Lin, J. Ren, and C. McGrath, “Mechanosensitive Piezo1 and Piezo2 ion channels in craniofacial development and dentistry: Recent advances and prospects,” *Frontiers in Physiology*, vol. 13, Oct. 2022, doi: 10.3389/fphys.2022.1039714.

[8] X. Peng, K. Dong, Z. Wu, J. Wang, and Z. L. Wang, “A review on emerging biodegradable polymers for environmentally benign transient electronic skins,” *Journal of Materials Science*, vol. 56, no. 30, pp. 16765–16789, Jul. 2021, doi: 10.1007/s10853-021-06323-0.

[9] S. Xu et al., “Force-induced ion generation in zwitterionic hydrogels for a sensitive silent-speech sensor,” *Nature Communications*, vol. 14, no. 1, Jan. 2023, doi: 10.1038/s41467-023-35893-7.

[10] Z. Chen and Y. Wang, “Ionic skin: from imitating natural skin to beyond,” *Industrial Chemistry & Materials*, vol. 1, no. 2, pp. 224–239, 2023, doi: 10.1039/d2im00062h.

[11] Y. Lin, J. Ren, and C. McGrath, “Mechanosensitive Piezo1 and Piezo2 ion channels in craniofacial development and dentistry: Recent advances and prospects,” *Frontiers in Physiology*, vol. 13, Oct. 2022, doi: 10.3389/fphys.2022.1039714.

[12] G. Seo et al., “Rapid Detection of COVID-19 Causative Virus (SARS-CoV-2) in Human Nasopharyngeal Swab Specimens Using Field-Effect Transistor-Based Biosensor,” *ACS Nano*, vol. 14, no. 4, pp. 5135–5142, Apr. 2020, doi: 10.1021/acsnano.0c02823.

[13] E. Caffrey, J. R. Garcia, D. O’Suilleabhain, C. Gabbett, T. Carey, and J. N. Coleman, “Quantifying the Piezoresistive Mechanism in High-Performance Printed Graphene Strain Sensors,” *ACS Applied Materials & Interfaces*, vol. 14, no. 5, pp. 7141–7151, Jan. 2022, doi: 10.1021/acsami.1c21623.

[14] A. S. Fiorillo, C. D. Critello, and S. A. Pullano, “Theory, technology and applications of piezoresistive sensors: A review,” *Sensors and Actuators A: Physical*, vol. 281, pp. 156–175, Oct. 2018, doi: 10.1016/j.sna.2018.07.006.

[15] J. Abot et al., “Foil Strain Gauges Using Piezoresistive Carbon Nanotube Yarn: Fabrication and Calibration,” *Sensors*, vol. 18, no. 2, p. 464, Feb. 2018, doi: 10.3390/s18020464.

[16] A. Shokuhfar, P. Heydari, M. R. Aliahmadi, M. Mohtashamifar, S. Ebrahimi-Nejad R., and M. Zahedinejad, “Low-cost polymeric microcantilever sensor with titanium as piezoresistive material,” *Microelectronic Engineering*, vol. 98, pp. 338–342, Oct. 2012, doi: 10.1016/j.mee.2012.07.067.

[17] A. Nag and S. C. Mukhopadhyay, “Fabrication and implementation of carbon nanotubes for piezoresistive-sensing applications: A review,” *Journal of Science: Advanced Materials and Devices*, vol. 7, no. 1, p. 100416, Mar. 2022, doi: 10.1016/j.jsamd.2021.100416.

[18] Y. Wan, Y. Wang, and C. F. Guo, “Recent progresses on flexible tactile sensors,” *Materials Today Physics*, vol. 1, pp. 61–73, Jun. 2017, doi: 10.1016/j.mtphys.2017.06.002.

[19] S. Chun, Y. Kim, H.-S. Oh, G. Bae, and W. Park, “A highly sensitive pressure sensor using a double-layered graphene structure for tactile sensing,” *Nanoscale*, vol. 7, no. 27, pp. 11652–11659, 2015, doi: 10.1039/c5nr00076a.

[20] B. Herren, V. Webster, E. Davidson, M. C. Saha, M. C. Altan, and Y. Liu, “PDMS Sponges with Embedded Carbon Nanotubes as Piezoresistive Sensors for Human Motion Detection,” *Nanomaterials*, vol. 11, no. 7, p. 1740, Jul. 2021, doi: 10.3390/nano11071740.

[21] C. Wang, L. Dong, D. Peng, and C. Pan, “Tactile Sensors for Advanced Intelligent Systems,” *Advanced Intelligent Systems*, vol. 1, no. 8, Sep. 2019, doi: 10.1002/aisy.201900090.

[22] L. Duan, D. R. D’hooge, and L. Cardon, “Recent progress on flexible and stretchable piezoresistive strain sensors: From design to application,” *Progress in Materials Science*, vol. 114, p. 100617, Oct. 2020, doi: 10.1016/j.pmatsci.2019.100617.

[23] Z. Ma, Y. Zhang, K. Zhang, H. Deng, and Q. Fu, “Recent progress in flexible capacitive sensors: Structures and properties,” *Nano Materials Science*, vol. 5, no. 3, pp. 265–277, Sep. 2023, doi: 10.1016/j.nanoms.2021.11.002.

[24] W. Chen and X. Yan, “Progress in achieving high-performance piezoresistive and capacitive flexible pressure sensors: A review,” *Journal of Materials Science & Technology*, vol. 43, pp. 175–188, Apr. 2020, doi: 10.1016/j.jmst.2019.11.010.

[25] S. Baek et al., “Flexible piezocapacitive sensors based on wrinkled microstructures: toward low-cost fabrication of pressure sensors over large areas,” *RSC Advances*, vol. 7, no. 63, pp. 39420–39426, 2017, doi: 10.1039/c7ra06997a.

[26] S. G. Yoon, B. J. Park, and S. T. Chang, “Highly Sensitive Piezocapacitive Sensor for Detecting Static and Dynamic Pressure Using Ion-Gel Thin Films and Conductive Elastomeric Composites,” *ACS Applied Materials & Interfaces*, vol. 9, no. 41, pp. 36206–36219, Oct. 2017, doi: 10.1021/acsami.7b11700.

[27] M. Pohanka, “Overview of Piezoelectric Biosensors, Immunosensors and DNA Sensors and Their Applications,” *Materials*, vol. 11, no. 3, p. 448, Mar. 2018, doi: 10.3390/ma11030448.

[28] S. Panda et al., “Piezoelectric energy harvesting systems for biomedical applications,” *Nano Energy*, vol. 100, p. 107514, Sep. 2022, doi: 10.1016/j.nanoen.2022.107514.

[29] B. H. Moghadam, M. Hasanzadeh, and A. Simchi, “Self-Powered Wearable Piezoelectric Sensors Based on Polymer Nanofiber–Metal–Organic Framework Nanoparticle Composites for Arterial Pulse Monitoring,” *ACS Applied Nano Materials*, vol. 3, no. 9, pp. 8742–8752, Aug. 2020, doi: 10.1021/acsanm.0c01551.

[30] N. A. Kamel, “Bio-piezoelectricity: fundamentals and applications in tissue engineering and regenerative medicine,” *Biophysical Reviews*, vol. 14, no. 3, pp. 717–733, Jun. 2022, doi: 10.1007/s12551-022-00969-z.

[31] K. Kapat, Q. T. H. Shubhra, M. Zhou, and S. Leeuwenburgh, “Piezoelectric Nano-Biomaterials for Biomedicine and Tissue Regeneration,” *Advanced Functional Materials*, vol. 30, no. 44, Feb. 2020, doi: 10.1002/adfm.201909045.

[32] J. Lu et al., “A Biodegradable and Recyclable Piezoelectric Sensor Based on a Molecular Ferroelectric Embedded in a Bacterial Cellulose Hydrogel,” *ACS Nano*, vol. 16, no. 3, pp. 3744–3755, Mar. 2022, doi: 10.1021/acsnano.1c07614.

[33] Q. Xu et al., “Bio-Piezoelectric Platforms: Construction of Bio-Piezoelectric Platforms: From Structures and Synthesis to Applications (Adv. Mater. 27/2021),” *Advanced Materials*, vol. 33, no. 27, Jul. 2021, doi: 10.1002/adma.202170206.

[34] T. Tat, A. Libanori, C. Au, A. Yau, and J. Chen, “Advances in triboelectric nanogenerators for biomedical sensing,” *Biosensors and Bioelectronics*, vol. 171, p. 112714, Jan. 2021, doi: 10.1016/j.bios.2020.112714.

[35] X. Pu, S. An, Q. Tang, H. Guo, and C. Hu, “Wearable triboelectric sensors for biomedical monitoring and human-machine interface,” *iScience*, vol. 24, no. 1, p. 102027, Jan. 2021, doi: 10.1016/j.isci.2020.102027.

[36] A. A. Mathew, A. Chandrasekhar, and S. Vivekanandan, “A review on real-time implantable and wearable health monitoring sensors based on triboelectric nanogenerator approach,” *Nano Energy*, vol. 80, p. 105566, Feb. 2021, doi: 10.1016/j.nanoen.2020.105566.

[37] G. Zhao et al., “Transparent and stretchable triboelectric nanogenerator for self-powered tactile sensing,” *Nano Energy*, vol. 59, pp. 302–310, May 2019, doi: 10.1016/j.nanoen.2019.02.054.

[38] H. Lei et al., “Self-Assembled Porous-Reinforcement Microstructure-Based Flexible Triboelectric Patch for Remote Healthcare,” *Nano-Micro Letters*, vol. 15, no. 1, Apr. 2023, doi: 10.1007/s40820-023-01081-x.

[39] D. W. Kim, J. H. Lee, J. K. Kim, and U. Jeong, “Material aspects of triboelectric energy generation and sensors,” *NPG Asia Materials*, vol. 12, no. 1, Jan. 2020, doi: 10.1038/s41427-019-0176-0.

[40] Y. Liu and C. Hu, “Triboelectric nanogenerators based on elastic electrodes,” *Nanoscale*, vol. 12, no. 39, pp. 20118–20130, 2020, doi: 10.1039/d0nr04868b.

[41] K. Chen and D. Ho, “Piezoionics: Mechanical-to-ionic transduction for sensing, biointerface, and energy harvesting,” *Aggregate*, Sep. 2023, Published, doi: 10.1002/agt2.425.

[42] M. Sarwar et al., “Transparent and Conformal ‘PiezoIonic’ Touch Sensor,” *Electroactive Polymer Actuators and Devices (EAPAD),* Apr. 2015, https://doi.org/10.1117/12.2085598

[43] Z. Zhao et al., “Recent Development of Self-Powered Tactile Sensors Based on Ionic Hydrogels,” *Gels*, vol. 9, no. 3, p. 257, Mar. 2023, doi: 10.3390/gels9030257.

[44] V. Woehling et al., “Study of the piezoionic effect and influence of electrolyte in conducting polymer based soft strain sensors,” *Multifunctional Materials*, vol. 2, no. 4, p. 045002, Dec. 2019, doi: 10.1088/2399-7532/ab56a2.

[45] Y. Dobashi et al., “Piezoionic mechanoreceptors: Force-induced current generation in hydrogels,” Science, vol. 376, no. 6592, pp. 502–507, Apr. 2022, doi: 10.1126/science.aaw1974.

[46] J. I. Lee et al., “Visco-Poroelastic Electrochemiluminescence Skin with Piezo-Ionic Effect,” *Advanced Materials*, vol. 33, no. 29, Jun. 2021, doi: 10.1002/adma.202100321.

[47] Y. Liu, Y. Hu, J. Zhao, G. Wu, X. Tao, and W. Chen, “Self-Powered Piezoionic Strain Sensor toward the Monitoring of Human Activities,” *Small*, vol. 12, no. 36, pp. 5074–5080, May 2016, doi: 10.1002/smll.201600553.

[48] R. Scaffaro, A. Maio, and M. C. Citarrella, “Ionic tactile sensors as promising biomaterials for artificial skin: Review of latest advances and future perspectives,” *European Polymer Journal*, vol. 151, p. 110421, May 2021, doi: 10.1016/j.eurpolymj.2021.110421.

[49] K. Saha, A. Chatterjee, A. Das, A. Ghorai, and U. Jeong, “Self-powered ionic tactile sensors,” *Journal of Materials Chemistry C*, vol. 11, no. 24, pp. 7920–7936, 2023, doi: 10.1039/d2tc05109e.

[50] T.-C. Ho et al., “Hydrogels: Properties and Applications in Biomedicine,” *Molecules*, vol. 27, no. 9, p. 2902, May 2022, doi: 10.3390/molecules27092902.

[51] F. Ullah, M. B. H. Othman, F. Javed, Z. Ahmad, and H. Md. Akil, “Classification, processing and application of hydrogels: A review,” *Materials Science and Engineering: C*, vol. 57, pp. 414–433, Dec. 2015, doi: 10.1016/j.msec.2015.07.053.

[52] D. Buenger, F. Topuz, and J. Groll, “Hydrogels in sensing applications,” *Progress in Polymer Science*, vol. 37, no. 12, pp. 1678–1719, Dec. 2012, doi: 10.1016/j.progpolymsci.2012.09.001.

[53] K. Elkhoury et al., “Soft-Nanoparticle Functionalization of Natural Hydrogels for Tissue Engineering Applications,” *Advanced Healthcare Materials*, vol. 8, no. 18, Aug. 2019, doi: 10.1002/adhm.201900506.

[54] F. Pinelli, L. Magagnin, and F. Rossi, “Progress in hydrogels for sensing applications: a review,” *Materials Today Chemistry*, vol. 17, p. 100317, Sep. 2020, doi: 10.1016/j.mtchem.2020.100317.

[55] W. Zhang, X. Jin, H. Li, R. Zhang, and C. Wu, “Injectable and body temperature sensitive hydrogels based on chitosan and hyaluronic acid for pH sensitive drug release,” *Carbohydrate Polymers*, vol. 186, pp. 82–90, Apr. 2018, doi: 10.1016/j.carbpol.2018.01.008.

[56] A. Guiseppi-Elie, “Electroconductive hydrogels: Synthesis, characterization and biomedical applications,” *Biomaterials*, vol. 31, no. 10, pp. 2701–2716, Apr. 2010, doi: 10.1016/j.biomaterials.2009.12.052.

[57] S. Brahim and A. Guiseppi-Elie, “Electroconductive Hydrogels: Electrical and Electrochemical Properties of Polypyrrole-Poly(HEMA) Composites,” *Electroanalysis*, vol. 17, no. 7, pp. 556–570, Apr. 2005, doi: 10.1002/elan.200403109.

[58] T.-S. Tsai et al., “A Polyvinyl Alcohol-Polyaniline Based Electro-Conductive Hydrogel for Controlled Stimuli-Actuable Release of Indomethacin,” *Polymers*, vol. 3, no. 1, pp. 150–172, Jan. 2011, doi: 10.3390/polym3010150.

[59] S. Liang et al., “Paintable and Rapidly Bondable Conductive Hydrogels as Therapeutic Cardiac Patches,” *Advanced Materials*, vol. 30, no. 23, Apr. 2018, doi: 10.1002/adma.201704235.

[60] H. Lu, N. Zhang, and M. Ma, “Electroconductive hydrogels for biomedical applications,” *WIREs Nanomedicine and Nanobiotechnology*, vol. 11, no. 6, Jun. 2019, doi: 10.1002/wnan.1568.

[61] H. Li, T. Lv, N. Li, Y. Yao, K. Liu, and T. Chen, “Ultraflexible and tailorable all-solid-state supercapacitors using polyacrylamide-based hydrogel electrolyte with high ionic conductivity,” *Nanoscale*, vol. 9, no. 46, pp. 18474–18481, 2017, doi: 10.1039/c7nr07424g.

[62] L. Zhang et al., “Overview of Ionogels in Flexible Electronics,” *The Chemical Record*, vol. 20, no. 9, pp. 948–967, Jul. 2020, doi: 10.1002/tcr.202000041.

[63] Z. Cao, H. Liu, and L. Jiang, “Transparent, mechanically robust, and ultrastable ionogels enabled by hydrogen bonding between elastomers and ionic liquids,” *Materials Horizons*, vol. 7, no. 3, pp. 912–918, 2020, doi: 10.1039/c9mh01699f.

[64] R. A. S. I. Subad, L. B. Cross, and K. Park, “Soft Robotic Hands and Tactile Sensors for Underwater Robotics,” *Applied Mechanics*, vol. 2, no. 2, pp. 356–383, Jun. 2021, doi: 10.3390/applmech2020021.

[65] Y. Zhou, B. He, Z. Yan, Y. Shang, Q. Wang, and Z. Wang, “Touch Locating and Stretch Sensing Studies of Conductive Hydrogels with Applications to Soft Robots,” Sensors, vol. 18, no. 2, p. 569, Feb. 2018, doi: 10.3390/s18020569.

[66] B. T. Phillips et al., “A Dexterous, Glove-Based Teleoperable Low-Power Soft Robotic Arm for Delicate Deep-Sea Biological Exploration,” *Scientific Reports*, vol. 8, no. 1, Oct. 2018, doi: 10.1038/s41598-018-33138-y.

[67] X. Zhou and P. S. Lee, “Three-dimensional printing of tactile sensors for soft robotics,” *MRS Bulletin*, vol. 46, no. 4, pp. 330–336, Apr. 2021, doi: 10.1557/s43577-021-00079-3.

[68] M. Ntagios, H. Nassar, A. Pullanchiyodan, W. T. Navaraj, and R. Dahiya, “Robotic Hands with Intrinsic Tactile Sensing via 3D Printed Soft Pressure Sensors,” *Advanced Intelligent Systems*, vol. 2, no. 6, Oct. 2019, doi: 10.1002/aisy.201900080.

[69] M. Ma et al., “Self-powered artificial electronic skin for high-resolution pressure sensing,” *Nano Energy*, vol. 32, pp. 389–396, Feb. 2017, doi: 10.1016/j.nanoen.2017.01.004.

[70] P. Roberts, M. Zadan, and C. Majidi, “Soft Tactile Sensing Skins for Robotics,” *Current Robotics Reports*, vol. 2, no. 3, pp. 343–354, Jul. 2021, doi: 10.1007/s43154-021-00065-2.

[71] S. J. Benight, C. Wang, J. B. H. Tok, and Z. Bao, “Stretchable and self-healing polymers and devices for electronic skin,” *Progress in Polymer Science*, vol. 38, no. 12, pp. 1961–1977, Dec. 2013, doi: 10.1016/j.progpolymsci.2013.08.001.

[72] A. Chortos, J. Liu, and Z. Bao, “Pursuing prosthetic electronic skin,” *Nature Materials*, vol. 15, no. 9, pp. 937–950, Jul. 2016, doi: 10.1038/nmat4671.

[73] Z. Huo et al., “Recent Advances in Large-Scale Tactile Sensor Arrays Based on a Transistor Matrix,” *Advanced Materials Interfaces*, vol. 5, no. 21, Sep. 2018, doi: 10.1002/admi.201801061.

[74] Z. Lou et al., “Ultrasensitive and ultraflexible e-skins with dual functionalities for wearable electronics,” *Nano Energy*, vol. 38, pp. 28–35, Aug. 2017, doi: 10.1016/j.nanoen.2017.05.024.

[75] C. Lu, X. Chen, and X. Zhang, “Highly Sensitive Artificial Skin Perception Enabled by a Bio-inspired Interface,” *ACS Sensors*, vol. 8, no. 4, pp. 1624–1629, Mar. 2023, doi: 10.1021/acssensors.2c02743.

[76] R. Dahiya, “E-Skin: From Humanoids to Humans [Point of View],” *Proceedings of the IEEE*, vol. 107, no. 2, pp. 247–252, Feb. 2019, doi: 10.1109/jproc.2018.2890729.

[77] Y.-L. Hsu, S.-C. Yang, H.-C. Chang, and H.-C. Lai, “Human Daily and Sport Activity Recognition Using a Wearable Inertial Sensor Network,” *IEEE Access*, vol. 6, pp. 31715–31728, 2018, doi: 10.1109/access.2018.2839766.

[78] J. Wang, C. Lu, and K. Zhang, “Textile-Based Strain Sensor for Human Motion Detection,” *ENERGY & ENVIRONMENTAL MATERIALS*, vol. 3, no. 1, pp. 80–100, Aug. 2019, doi: 10.1002/eem2.12041.

[79] X. Wu, Y. Han, X. Zhang, and C. Lu, “Highly Sensitive, Stretchable, and Wash-Durable Strain Sensor Based on Ultrathin Conductive Layer@Polyurethane Yarn for Tiny Motion Monitoring,” *ACS Applied Materials & Interfaces*, vol. 8, no. 15, pp. 9936–9945, Apr. 2016, doi: 10.1021/acsami.6b01174.

[80] J. Zhang et al., “Human motion monitoring in sports using wearable graphene-coated fiber sensors,” *Sensors and Actuators A: Physical*, vol. 274, pp. 132–140, May 2018, doi: 10.1016/j.sna.2018.03.011.

[81] Y. Liu et al., “Thin, Skin-Integrated, Stretchable Triboelectric Nanogenerators for Tactile Sensing,” *Advanced Electronic Materials*, vol. 6, no. 1, Nov. 2019, doi: 10.1002/aelm.201901174.

[82] Y. Yang et al., “Stretchable Energy-Harvesting Tactile Interactive Interface with Liquid-Metal-Nanoparticle-Based Electrodes,” *Advanced Functional Materials*, vol. 30, no. 29, Jan. 2020, doi: 10.1002/adfm.201909652.

[83] V. Vallem, Y. Sargolzaeiaval, M. Ozturk, Y. Lai, and M. D. Dickey, “Energy Harvesting and Storage: Energy Harvesting and Storage with Soft and Stretchable Materials (Adv. Mater. 19/2021),” *Advanced Materials*, vol. 33, no. 19, May 2021, doi: 10.1002/adma.202170151.

[84] M. Caprioli, I. Roppolo, A. Chiappone, L. Larush, C. F. Pirri, and S. Magdassi, “3D-printed self-healing hydrogels via Digital Light Processing,” *Nature Communications*, vol. 12, no. 1, Apr. 2021, doi: 10.1038/s41467-021-22802-z.

[85] Y. Marcus, “Thermodynamics of solvation of ions. Part 5.—Gibbs free energy of hydration at 298.15 K,” J. Chem. Soc., Faraday Trans., vol. 87, no. 18, pp. 2995–2999, 1991, doi: 10.1039/ft9918702995.